

# Sustainable management of groundwater resources in the Maghreb

Estimation of groundwater use for  
agricultural purpose based on remote  
sensing data



Bundesanstalt für  
Geowissenschaften  
und Rohstoffe



Bundesanstalt für  
Geowissenschaften  
und Rohstoffe



german  
cooperation  
DEUTSCHE ZUSAMMENARBEIT



OBSERVATOIRE DU SAHARA ET DU SAHEL  
SAHARA AND SAHEL OBSERVATORY

Authors: Fabian Stoffner and Dr. Clémence Dubois  
Federal Institute of Geosciences and Natural Resources (BGR),  
Remote Sensing Unit, Hanover, Germany

Project: Regional cooperation for a sustainable groundwater management in  
the Maghreb region (Algeria, Morocco, Tunisia) I & II

Commissioned by: Federal Ministry for Economic Cooperation and Development  
(BMZ), Germany

BMZ Project Numbers: 2013.2289.0 (I) & 2017.2213.1 (II)

BGR Project Number: 05-2369

Date: January 2021

To be cited as: Stoffner, F. and Dubois, C. (2021): Sustainable management of  
groundwater resources in the Maghreb - Estimation of groundwater  
use for agricultural purpose based on remote sensing data. BGR  
Project Number: 05-2369.

To be found: Online in the BGR library and on the project websites of the BGR  
[www.bgr.bund.de/EN](http://www.bgr.bund.de/EN)

## Content

Content .....	III
Abbreviations .....	V
List of figures .....	VI
List of tables .....	VIII
1 Scope of work .....	1
2 Working Areas.....	2
3 Tunisia .....	3
3.1 Optical Processing – SPOT and RapidEye.....	3
3.1.1 Data .....	4
3.1.2 Methodology .....	5
3.1.3 Results .....	6
3.2 Optical Processing – Sentinel 2.....	8
3.2.1 Data .....	8
3.2.2 Methodology .....	10
3.2.3 Results .....	13
3.3 RADAR Processing.....	18
3.3.1 Data .....	18
3.3.2 Methodology .....	18
3.3.3 Results and Interpretation .....	19
3.4 Transfer to DSS .....	38
3.4.1 Data .....	38
3.4.2 Methodology .....	38
3.4.3 Results .....	40
4 Algeria.....	41
4.1 Inventory of groundwater abstraction points .....	41
4.2 Optical Processing .....	41
4.2.1 Data .....	41
4.2.2 Methodology .....	42
4.2.3 Results .....	43
4.3 RADAR Processing.....	46
4.3.1 Data .....	46

4.3.2	Methodology .....	47
4.3.3	Results and Interpretation .....	47
5	Morocco .....	50
6	Representation of the project .....	51
6.1	Supervision of Internship students.....	51
6.2	Training of OSS.....	51
6.3	Attendance of conferences.....	51
6.4	Publications.....	52
7	Conclusions and future work .....	53
8	References.....	54

## Abbreviations

<b>ABH CSM</b>	Agence de Bassin Hydrographique Constantinois - Seybousse - Mellegue
<b>ASAR</b>	Advanced Synthetic Aperture Radar
<b>BGR</b>	Federal Institute of Geosciences and Natural Resources
<b>BMZ</b>	Federal Ministry for Economic Cooperation and Development
<b>CCI</b>	Climate Change Initiative
<b>DEM</b>	Digital Elevation Model
<b>DRE</b>	Direction de Ressources en Eau
<b>DSA</b>	Direction des Superficies Agricoles
<b>DS</b>	Distributed Scatterer
<b>DSS</b>	Decision Support System
<b>EMD</b>	Emergence Date
<b>ENVISAT</b>	Environmental Satellite
<b>ESA</b>	European Space Agency
<b>FAO</b>	Food and Agriculture Organization
<b>INAT</b>	National Agronomic Institute of Tunisia
<b>Kc</b>	Crop coefficient
<b>Kcb</b>	Basal crop coefficient
<b>Ke</b>	Evaporation coefficient
<b>LOS</b>	Line Of Sight
<b>MD</b>	Minimum Distance
<b>ML</b>	Maximum Likelihood
<b>NDVI</b>	Normalized Difference Vegetation Index
<b>OSS</b>	Sahara and Sahel Observatory
<b>PP</b>	Parallel Piped
<b>PS</b>	Persistent Scatterer
<b>PSI</b>	Persistent Scatterer Interferometry
<b>RADAR</b>	Radio Detection And Ranging
<b>SAR</b>	Synthetic Aperture Radar
<b>SBAS</b>	Small Baseline Subset
<b>SPOT</b>	Satellite Pour l'Observation de la Terre
<b>SRTM</b>	Shuttle Radar Topography Mission
<b>SVM</b>	Support Vector Machine
<b>TDM</b>	Time Division Multiplexing
<b>WEAP</b>	Water Evaluation And Planning

## List of figures

<b>Figure 1:</b> Overview of the pilot areas .....	2
<b>Figure 2:</b> Detailed characteristics of the pilot areas; source of background: Google Earth....	2
<b>Figure 3:</b> Overlay of the ground truth data and the satellite data (SPOT, RGB, August 2015) .....	5
<b>Figure 4:</b> Supervised classification ML, Zoom (RapidEye, May 2016) .....	6
<b>Figure 5:</b> Supervised classification, MD (RapidEye, December 2015) .....	7
<b>Figure 6:</b> Chili pepper in August 2017.....	8
<b>Figure 7:</b> Pomegranate trees in August 2017 .....	9
<b>Figure 8:</b> Olive trees in April 2017.....	9
<b>Figure 9:</b> Overall workflow of the crop mapping approach .....	11
<b>Figure 10:</b> Principal crop classes and their respective macro-class .....	11
<b>Figure 11:</b> Multi-temporal NDVI profiles for a) winter 2016/2017 and b) summer 2017 .....	12
<b>Figure 12:</b> Schematic representation of the different multi-temporal features .....	13
<b>Figure 13:</b> Classification results; classification performed for winter on the acquisition from 05.03.2017 and for summer on the acquisition from 19.08.2017, Sentinel 2 tile SNE, dates providing the best separability between the classes according to the NDVI profiles. ....	15
<b>Figure 14:</b> a) Map of the emergence date winter 2016/ 2017 and b), c) water need maps for March 2017, Sentinel 2 tile SNE .....	17
<b>Figure 15:</b> Ground motion map for PSI on Sentinel 1 data.....	20
<b>Figure 16:</b> Ground motion map for SBAS on TerraSAR-X data .....	20
<b>Figure 17:</b> Ground motion map for SBAS on Sentinel 1 ascending data.....	21
<b>Figure 18:</b> Ground motion map for SBAS on Sentinel 1 decending data.....	21
<b>Figure 19:</b> Ground motion map for SBAS on ENVISAT ASAR data .....	22
<b>Figure 20:</b> a) Velocity map from PSI processing for the region of Nebhana; b) Velocity map from SBAS processing for the region of Nebhana; .....	23
<b>Figure 21:</b> a) Velocity map from Envisat ASAR SBAS processing for the region of Nebhana; b) Velocity map from Sentinel 1 SBAS processing for the region of Nebhana; both processing are performed with descending datasets. ....	25
<b>Figure 22:</b> Velocity map from Envisat ASAR SBAS processing for the region of Nebhana and superimposed piezometer locations. The piezometers selected for further interpretation are encircled in color .....	26
<b>Figure 23:</b> Ground water level (x) and corresponding displacement (•) at the different selected piezometers locations.....	27

<b>Figure 24:</b> a) Velocity map from TerraSAR-X SBAS processing for the region of Nebhana; b) Velocity map from Sentinel 1 SBAS processing for the region of Nebhana; both processings are performed with ascending datasets. ....	28
<b>Figure 25:</b> a) Vertical velocity from Sentinel 1 SBAS processing; b) Eastward velocity from Sentinel 1 SBAS processing.....	29
<b>Figure 26:</b> Vertical velocity from Sentinel 1 SBAS processing superimposed with a) delimitation of the aquifers; b) cropland mask; c) ground water wells; d) DEM (TanDEM-X).31	
<b>Figure 27:</b> a) Vertical velocity from Sentinel 1 SBAS processing superimposed with the delimitation of the geological and lithological units; b) corresponding geological map; c) corresponding lithological map. ....	33
<b>Figure 28:</b> a) Zoom to Sentinel 1 SBAS processing; b) corresponding satellite image; c) building in the centre of the deformation cluster; d) corresponding time series of main subsidence.....	34
<b>Figure 29:</b> Multitemporal optical imagery (Google Earth 2018) .....	35
<b>Figure 30:</b> a) Geographical location of the piezometers from Sentinel 1 SBAS processing; b) evolution of the groundwater level for selected piezometers (2015-2017); c) evolution of the groundwater level for selected piezometers (since 1973); d) corresponding ground motion .37	
<b>Figure 31:</b> Digitised olive tree layer.....	39
<b>Figure 32:</b> Schematic illustration of the components of the DSS.....	39
<b>Figure 33:</b> Crop type classification for the DSS.....	40
<b>Figure 34:</b> Workflow for the processing of the Algerian sites.....	43
<b>Figure 35:</b> a) external data- blue: water mask, green: forest mask; b) standard deviation of NDVI over the year 2017; c) resulting cropland mask after thresholding.....	44
<b>Figure 36:</b> NDVI Profiles for the year 2017 for four different crop types in Algeria. ....	45
<b>Figure 37:</b> Classification map and confusion matrix of the maximum likelihood classification for the plain of Remila.....	46
<b>Figure 38:</b> SBAS result for the plain of Remila, Algeria, on Sentinel 1 ascending data. ....	47
<b>Figure 39:</b> Considered areas for the analysis. ....	48
<b>Figure 40:</b> Zoom-up on selected areas and wells identification; source of optical imagery: Google Earth.....	48
<b>Figure 41:</b> Closer look on presumed wells; source of optical imagery: Google Earth .....	49

## List of tables

<b>Table 1:</b> Overview of the acquired SPOT and RapidEye data .....	4
<b>Table 2:</b> Overview of the recorded ground truth data 2015 and 2016.....	4
<b>Table 3:</b> Overview of the acquired Sentinel-2 data and ground truth .....	10
<b>Table 4:</b> Number of available acquisitions and time span for each considered sensor .....	18
<b>Table 5:</b> Method used for the processing of the different data.....	19
<b>Table 6:</b> Principal processing parameters for the different datasets .....	19
<b>Table 7:</b> Land use classes for the DSS .....	39
<b>Table 8:</b> Overview of the acquired Sentinel-2 data .....	42
<b>Table 9:</b> Number of available acquisitions and time span for each considered sensor .....	47



## 1. Scope of work

The Federal Institute of Geosciences and Natural Resources (BGR) and the Sahara and Sahel Observatory (OSS) are implementing a regional project for an improved groundwater management in the Maghreb region. Participating countries are Algeria, Morocco and Tunisia. The project is commissioned by the Federal Ministry for Economic Cooperation and Development (BMZ) with a total duration of 7 years (January 2014 – December 2020).

Among others, this regional cooperation in the water sector in the Maghreb aims at supporting regional authorities in obtaining qualitative and quantitative information about the use of water for agricultural purposes, with the sake of a sustainable regional ground water management. Within this project, the role of the BGR is to assist the regional organizations for collecting and interchanging relevant hydrogeological information, and to provide modern and efficient methods for estimating and monitoring groundwater conditions. An important aspect is also the training of the regional administrations, which should ensure a sustainable ground water management.

The remote sensing department of the BGR intercedes in this project with the utilization of multispectral and RADAR remote sensing data in order to estimate and monitor the water needs mainly for agricultural purpose. In particular, land cover and crop type classifications using optical remote sensing data are performed and land subsidence using RADAR remote sensing data is determined. The first one aiming parameter retrieval for the calculation of water requirements for agricultural use and the second aiming the awareness and quantification of the ground water discharge for agricultural purpose.

This report aims at describing the main technical activities including their results realised in the context of this cooperation by the remote sensing department of the BGR until June 2020.

## 2. Working Areas

The regional aspect of the project implies the choice of several pilot areas located in the different countries involved in the project. Depending on the specific starting points/baselines, the quantity and quality of available information, as well as the opportunity of acquiring new information, the national authorities choose the following regions as pilot areas see Figures 1 and 2.

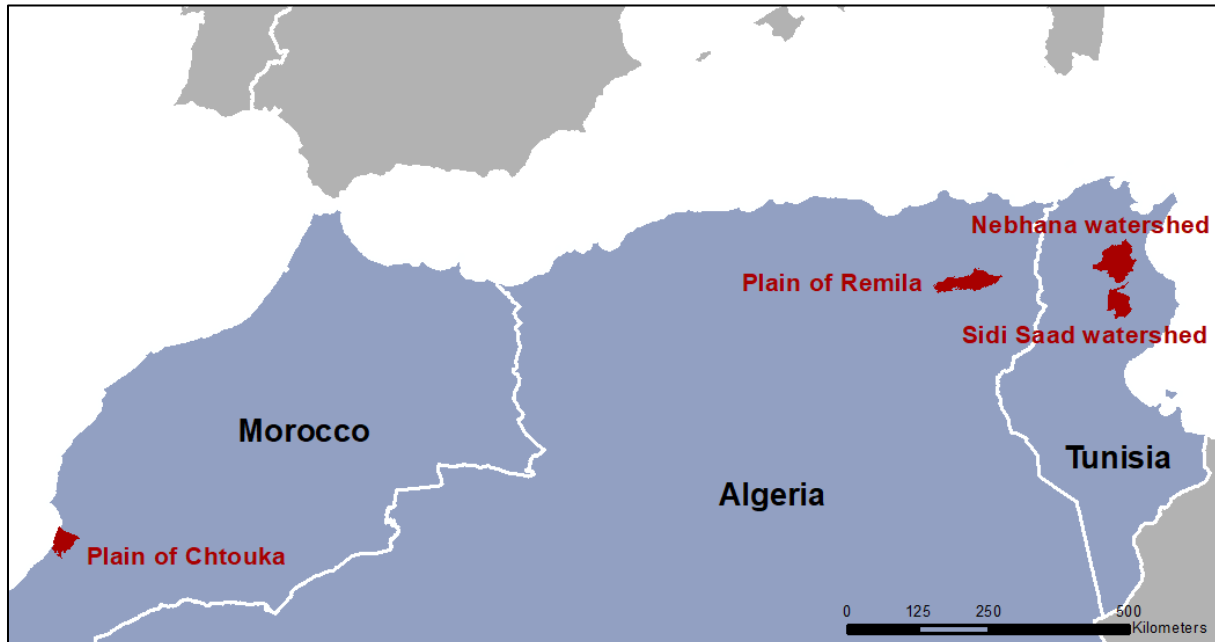


**Figure 1:** Overview of the pilot areas

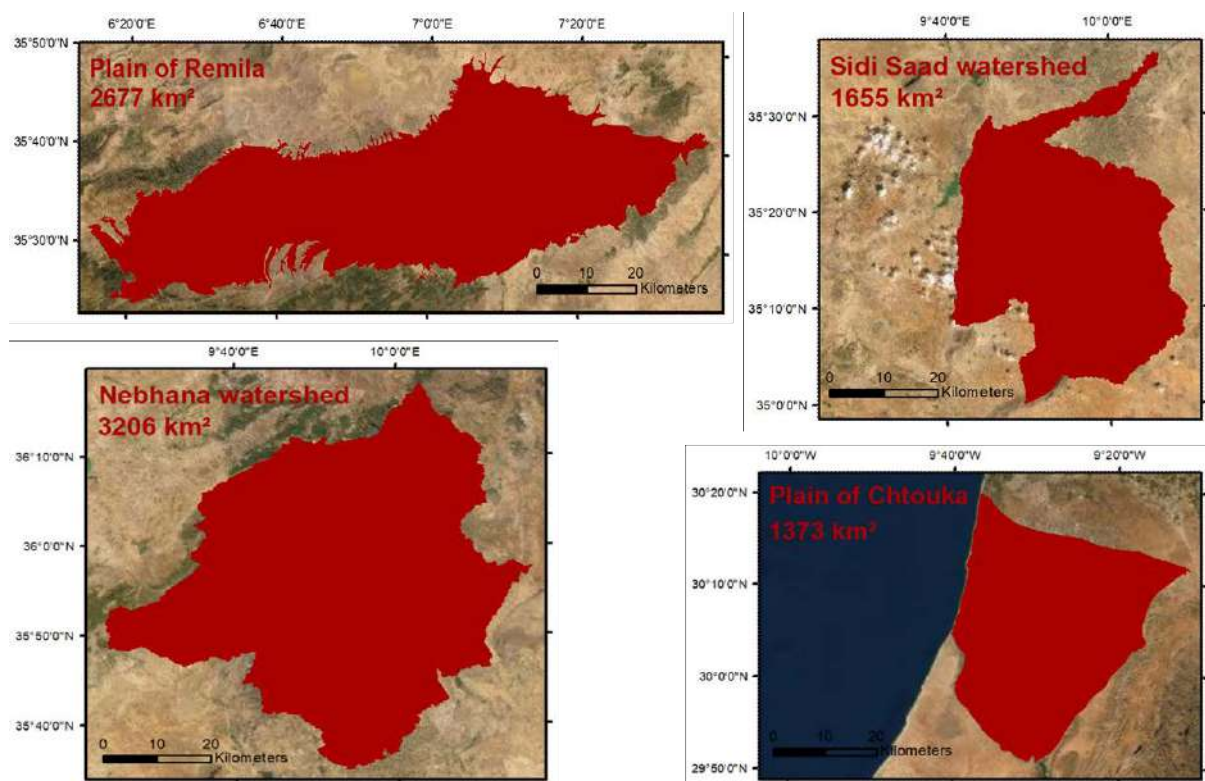


**Figure 2:** Detailed views of the pilot areas; source of background: Google Earth

### 3. Tunisia

In Tunisia, there are two pilot areas, the Nebhana watershed and the Sidi Saad watershed. The remote sensing based analyses and products are tested and performed for these two regions, whereby the Nebhana region was more in focus due to its importance for local water authorities. The final goal is the quantification of groundwater volumes used for agricultural purposes based on remote sensing analyses and the increase of awareness about the overexploitation of the underlying aquifer systems. Three methods have been investigated:

- (1) Land cover classification of multispectral SPOT and RapidEye data (chapter 3.1: Optical processing – SPOT and RapidEye)

Commercial satellite data were acquired in order to test several approaches for crop classification. This data are used to test the suitability for land cover discrimination in the study areas in terms of spatial and temporal resolution, especially in comparison to and for the rating of the Copernicus Sentinel 2 free and open data that perform lower spatial but high multitemporal resolution.

- (2) Land cover classification using multitemporal and multispectral Sentinel 2 data in order to estimate indirectly the crop evapotranspiration and the crop water needs (chapter 3.2: Optical processing – Sentinel 2)

Since Sentinel 2 data have been available from the European Space Agency (ESA), this data are used in a later stage of the project. This satellite data are based on a free and open data policy and, thus, guarantees financial sustainability for data acquisition. In addition, the spatial and temporal characteristics are found appropriate for land use classifications.

- (3) Estimation of land subsidence and uplift using RADAR data in order to correlate with ground water discharge (chapter 3.3: RADAR processing)

RADAR analyses may be an alternative to the use of optical data. It is an approach that measures the ground motion of the earth's surface. These results are then compared with the evolution of groundwater levels and pumping rates. Commercial data (TerraSAR) as well as Sentinel 1 RADAR data, which are based on a free and open data policy, have been used.

In addition, another objective of the project is the development of a decision support system (DSS) for the Nebhana water system. The DSS combines all aspects regarding the water cycle such as the drinking water supply, the surface runoff or the impacts on the hydrogeological system with the aim to facilitate the decision maker's daily work. Therefore, the approach of the optical processing is used in order to classify the land use for the DSS:

- (4) Land cover classification using multispectral Sentinel 2 data in order to integrate the results in the DSS (chapter 3.4: Transfer to DSS)




#### 3.1 Optical Processing – SPOT and RapidEye

This chapter shows the analyses of high spatial resolution data performed in order to classify the different crop types for the Nebhana region using satellite data at three single dates

### 3.1.1 Data

For the study area, commercial satellite data (SPOT 6/7 and RapidEye) are acquired at three different dates in order to perform land cover classifications and to identify the agricultural dynamics (Table 1). These dates are chosen according to the crop calendar and to allow an overview of all the crops grown during on year. Sewing and harvesting times depend on the crop types and therefore must be considered.

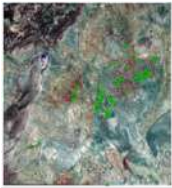
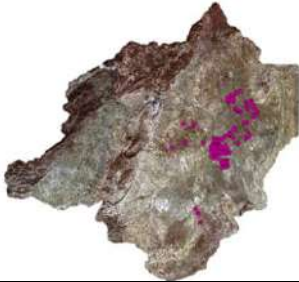

**Table 1:** Overview of the acquired SPOT and RapidEye data

			
Region	Nebhana watershed, part	Nebhana watershed, complete	Nebhana watershed, complete
Surface	2,743 km <sup>2</sup>	3,446 km <sup>2</sup>	3,446 km <sup>2</sup>
Satellite	SPOT 6/7	RapidEye	SPOT 6/7
Recording date	August 2015	December 2015	May 2016
Spatial resolution	5 m	6 m	5 m
Spectral resolution	4 bands + pan	5 bands	4 bands + pan
Costs	6,309 €	5,427 €	7,926 €

Pre-processing steps including atmospheric correction for comparison of different acquisition dates are performed for all data.

The National Agronomic Institute of Tunisia (INAT) that was subcontracted by the project carried out Field surveys during the record periods of the satellite data (Table 2). Information about the crop types for several land plots are collected. This ground truth data are necessary to compare and validate the information coming from the satellite data.

**Table 2:** Overview of the recorded ground truth data 2015 and 2016

			
Satellite	SPOT 6/7	RapidEye	SPOT 6/7
Recording date	August 2015	December 2015	May 2016
Number of plots	117	310	157
Number of crop types	23	40	23



The land plots of the field surveys are not the same for each date. For instance, in December 2015 different land plots were recorded than in August 2015. Thus, an analysis of the evolution of single plots over the time is not possible. The ground truth data can only be used as a reference for each single date. In addition, the ground truth data are partly incorrect in terms of crop type determination in the field or information of the land plot sometimes cannot be assigned clearly to the satellite data. The reason for this is that project staff and partners changed and the continuity was not guaranteed. Furthermore, most of the fieldwork was realised by university students that were not all sufficiently experienced. These aspects were a disadvantage for the data analysis, which has been improved in the further project work.

### 3.1.2 Methodology

The available ground truth data are analysed to understand the agricultural activities in the project area. Thus, information about the variety of crop types and the corresponding growing period (winter or summer season) are figured out. In August 2015 and in May 2016 23 crop types are identified, whereas in December 2015 40 crop types are specified (Table 2).

The different crop types are then matched with the satellite data in order to determine their spectral reflectance as well as their spectral separability characteristics (Figure 3). This step is necessary to see how well the crop types can be distinguished and whether they can be separated from each other. If the spectral reflectance characteristics of two (or more) crop types, which grow during the same period, is too similar a separation is not possible.

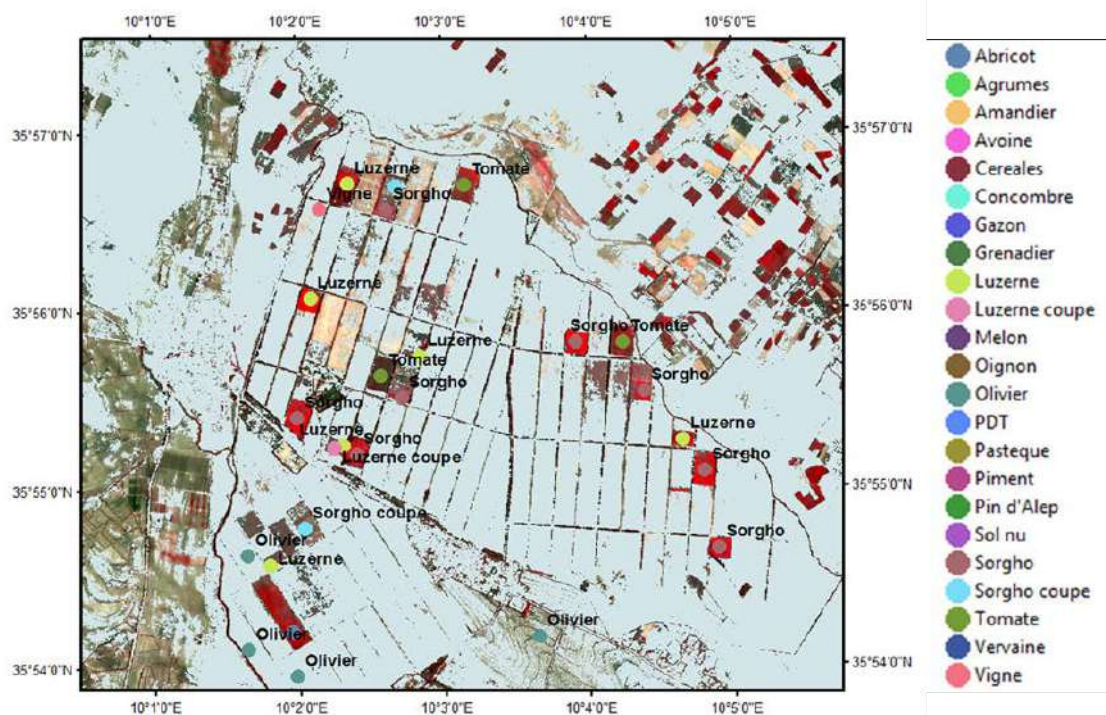


**Figure 3:** Overlay of the ground truth data and the satellite data (SPOT, RGB, August 2015)

Using the ground truth data several supervised image classifications considering all single crop types as classes are performed for each date. This includes minimum distance (MD), maximum likelihood (ML), parallel-piped (PP) and support vector machine (SVM) classifications.

In addition, in order to simplify the analysis and to compare the results, the single crop types are merged into crop classes. The criteria to build a crop class are the spectral reflectance and

the growing period. Thus, a crop class includes single crop types with similar spectral reflectance at the same date. The tested classes are *cropland*, *urban areas*, *water bodies*, *wooden areas* and *bare soil*. Then, a supervised classification is performed in order to assess the separability of the merged classes and especially of the agricultural areas.

### 3.1.3 Results

The separability analyses of the ground truth data for the three dates show that there are several similarities between the different crop types regarding the spectral reflectance and that the high number of single crop types cannot be distinguished in the remote sensing data with the available ground truth data. In addition, the same crop types may have different planting dates and, thus, the growing period may be different. That means also that different growing stages of the same crop type can be observed for the same date. Accordingly, the spectral reflectance of a specific crop type may vary on different land plots. The performed classifications show corresponding results. The different land plots contain not only one crop type as it should be, but a large number of different crop types as it is shown exemplary in Figure 4. An overview of a supervised classification (RapidEye, December 2015) for the whole project area is given in Figure 5.

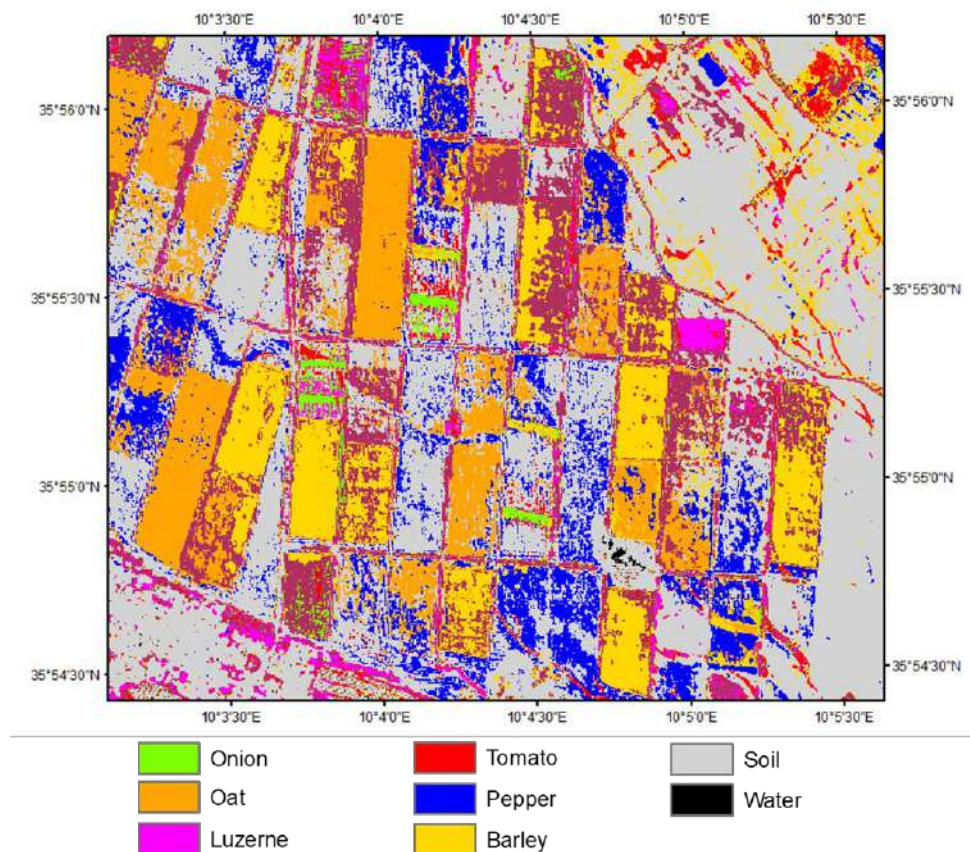


**Figure 4:** Supervised classification ML, Zoom (RapidEye, May 2016)



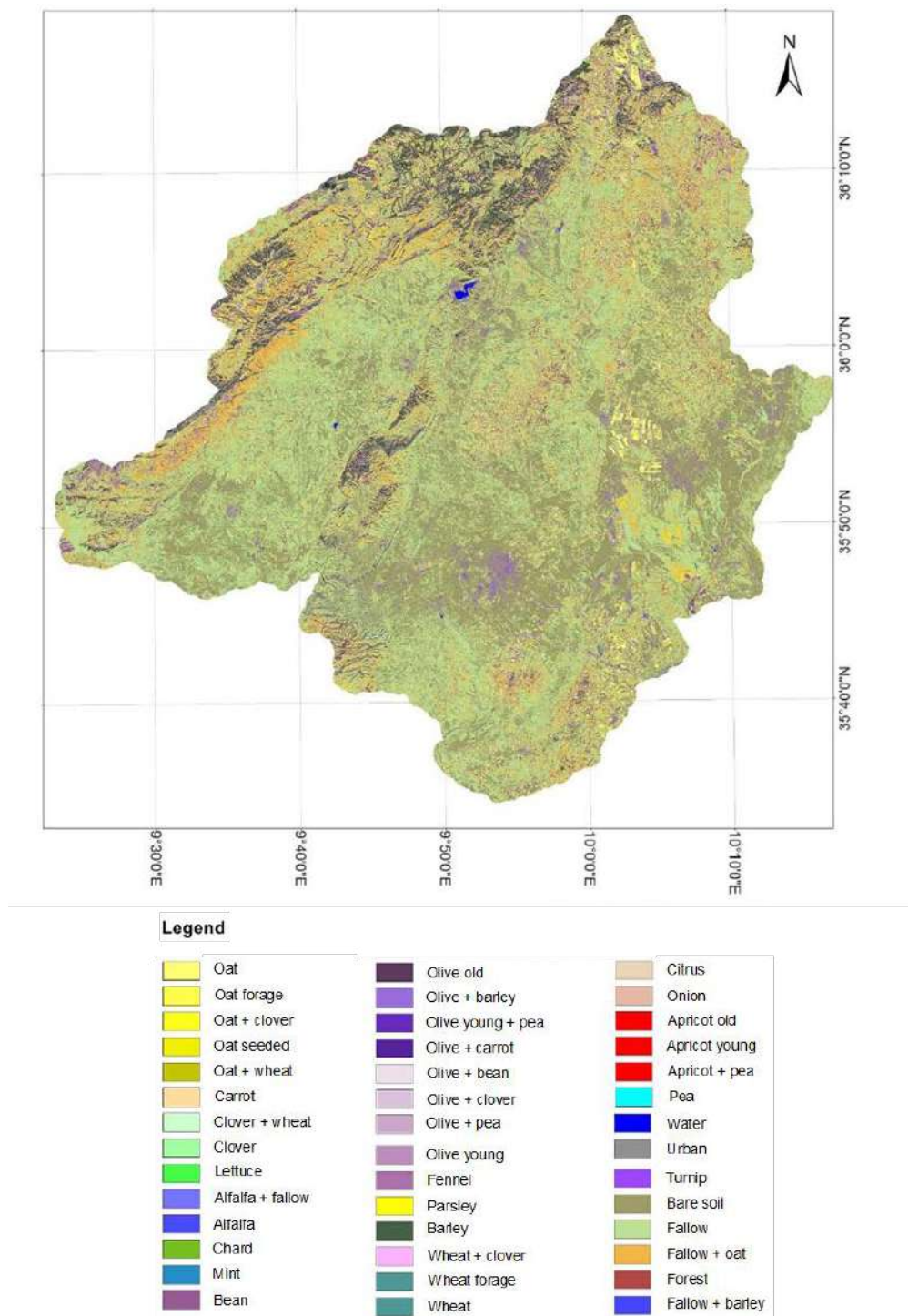


**Figure 5:** Supervised classification, MD (RapidEye, December 2015)

However, agricultural areas and their crop types compared to non-agricultural areas like urban areas, bare soil and water bodies can be well separated by using classifications and crop classes training sites. Confusion may occur between agricultural areas, especially tree crops, and wooded areas. Wooded areas in the study area have a low density, as it is the case for tree crop plantations.

Due to the available ground truth data and the partly incorrect information, the use of the data is limited. Therefore, the calculation based on this training data as well as the quality is biased. Information about the crop types and their evolution over the time that are more reliable may lead to results that are more robust. Then, also, an independent validation based on additional ground truth data is necessary in order to evaluate the quality of the classifications.

A higher temporal and spectral resolution of satellite data would be an advantage. Since 2015, the Copernicus Program of the European Commission in partnership with the ESA offers with its SENTINEL mission high temporal resolution and advanced spectral resolution satellite imagery that are available for everyone based on a free and open data policy. Combined with a solid database of ground truth information, this data are expected to allow a more detailed and reliable satellite based crop monitoring.

## 3.2 Optical Processing – Sentinel 2

This part presents the methodology developed for land cover classification and subsequent determination of crop water need for Tunisia using Sentinel 2 data. Most of the following sub-sections are based on (Dubois et al., 2018).

### 3.2.1 Data

For the study, the water needs of the region for two different agricultural seasons are analysed, i.e. winter 2016/2017 and summer 2017. The winter season in Tunisia lasts generally from October to April, and the summer season from May to September. Important crops during winter are cereals, forages, small vegetables (mostly peas) and tree plantations. In summer, only vegetables, trees and some forages are relevant for the water balance. The developed methodology aims at performing land use classification using multi-temporal information in order to better distinguish the different crop types.



**Figure 6:** Chili pepper in August 2017





**Figure 7:** Pomegranate trees in August 2017



**Figure 8:** Olive trees in April 2017

Free and open, available Copernicus data of Sentinel-2 are used in order to obtain a regular and high temporal coverage of the area for following the evolution of the different crop types. The considered acquisitions and respective ground truth data are listed in Table 3. For the winter season, all available cloud free images have been considered, whereas for the summer season, only one cloud-free dataset per month is considered - corresponding to the date of the specific ground truth campaigns - in order to keep the computation time low. As mentioned earlier, especially in summer in this region, less distinct crop types are expected as in winter, allowing a multi-temporal analysis of the different crop types based on a monthly data rate.

In order to obtain sufficient reference and to perform a detailed temporal analysis of the different crop types, monthly ground truth data were acquired, in order to analyse the specific evolution of the different cultures over the region. In total, 357 reference plots are observed and monitored each month, for a total area of 1221 km<sup>2</sup> and an agricultural area of 481 km<sup>2</sup>. The mentioned area is smaller than the whole study area as for the development of the methodology, only one Sentinel 2 tile was considered in order to keep computation time low. The area correspond therefore to the mapped area in a single Sentinel 2 tile (tile SNE). However, the methodology is replicable for larger areas. As the ground truth data are acquired considering 55 different crop types (subclasses), each crop type is only represented by a few plots. Therefore, in order to ensure a good and reliable result, the classifier is trained with 70% of the ground truth data and the validation is based on 30% of the ground truth data.

**Table 3:** Overview of the acquired Sentinel-2 data and ground truth

Ground Truth	Sentinel-2 acquisitions for winter crops	Sentinel-2 acquisitions for summer crops
Nov. 2016 week 46	03.10.2016	
	06.10.2016	
	18.10.2016	
	28.10.2016	
	25.11.2016	
Dec. 2016 week 52	02.12.2016	
	01.01.2017	
Jan. 2017 week 4	24.01.2017	
	31.01.2017	
	03.02.2017	
Feb. 2017 week 8	23.02.2017	
	02.03.2017	
	05.03.2017	
Mar. 2017 week 12-13	12.03.2017	
	01.04.2017	
Apr. 2017 week 17-18	14.04.2017	
	24.04.2017	24.04.2017
	01.05.2017	
May 2017 week 21-22		24.05.2017
		13.06.2017
July 2017 week 27		13.07.2017
Aug. 2017 week 31-32		19.08.2017
Sept. 2017 week 37-38		21.09.2017
		18.10.2017

### 3.2.2 Methodology

The methodological workflow is shown in Figure 9. Considering a stack of Sentinel-2 data for one season, the data are first pre-processed in order to correct atmosphere and relief influence, and a cropland mask is used in order to consider only the agricultural areas for further processing steps. In order to focus on the specific water need for agricultural use, the Cropland mask of the ESA CCI land cover – S2 prototype land cover 20m map of Africa 2016 (CCI Land Cover, 2017) is used, which is well defined for the test area. In a second step, the NDVI is calculated for each dataset. Based on the acquired ground truth data and the NDVI time series, NDVI profiles for the different crop types are calculated. Five macro-classes are considered based on the consolidated 55 crop subclasses: cereals, forages, trees, vegetables and bare soil. Those five macro-classes are identified as corresponding to specific differing water needs following FAO (Allen, 1998).

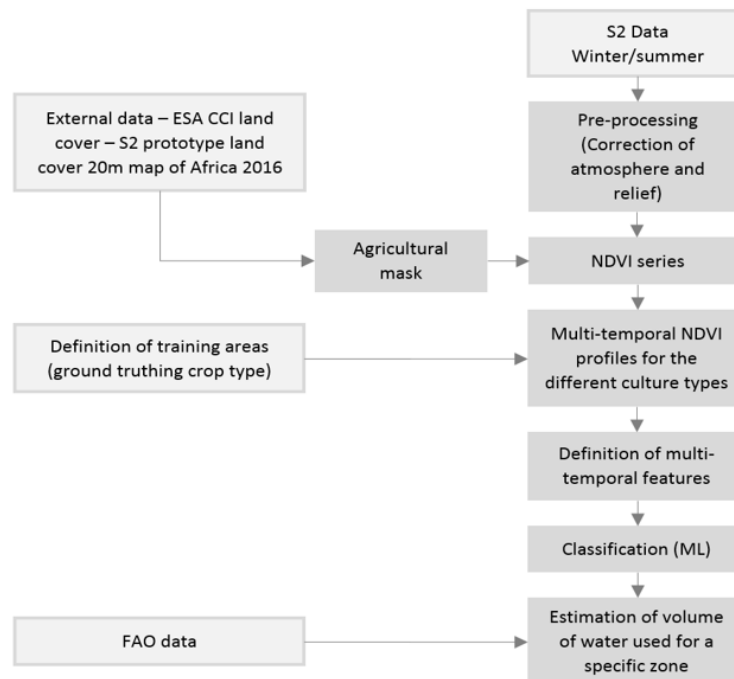


**Figure 9:** Overall workflow of the crop mapping approach

Figure 10 shows an overview of the principal subclasses regrouped in those macro-classes for each season. The subclasses of one macro-class mostly have very similar water needs, during the same period. For each macro-class, the mean NDVI is calculated using the corresponding ground truth data (Table 3). The resulting profiles are represented in Figure 11a and b for the winter and summer season, respectively.

Macro-class	Principal subclasses winter	Principal subclasses summer
Trees	Olive tree	Olive tree
		Apricot tree
		Citrus trees
Cereals	Oat	
	Wheat	
	Barley	
Forages	Clover	Clover
	Green barley	
Vegetables	Peas	Peas
	Beans	Watermelon
		Pepper
Bare soil	Bare soil, straw	

**Figure 10:** Principal crop classes and their respective macro-class

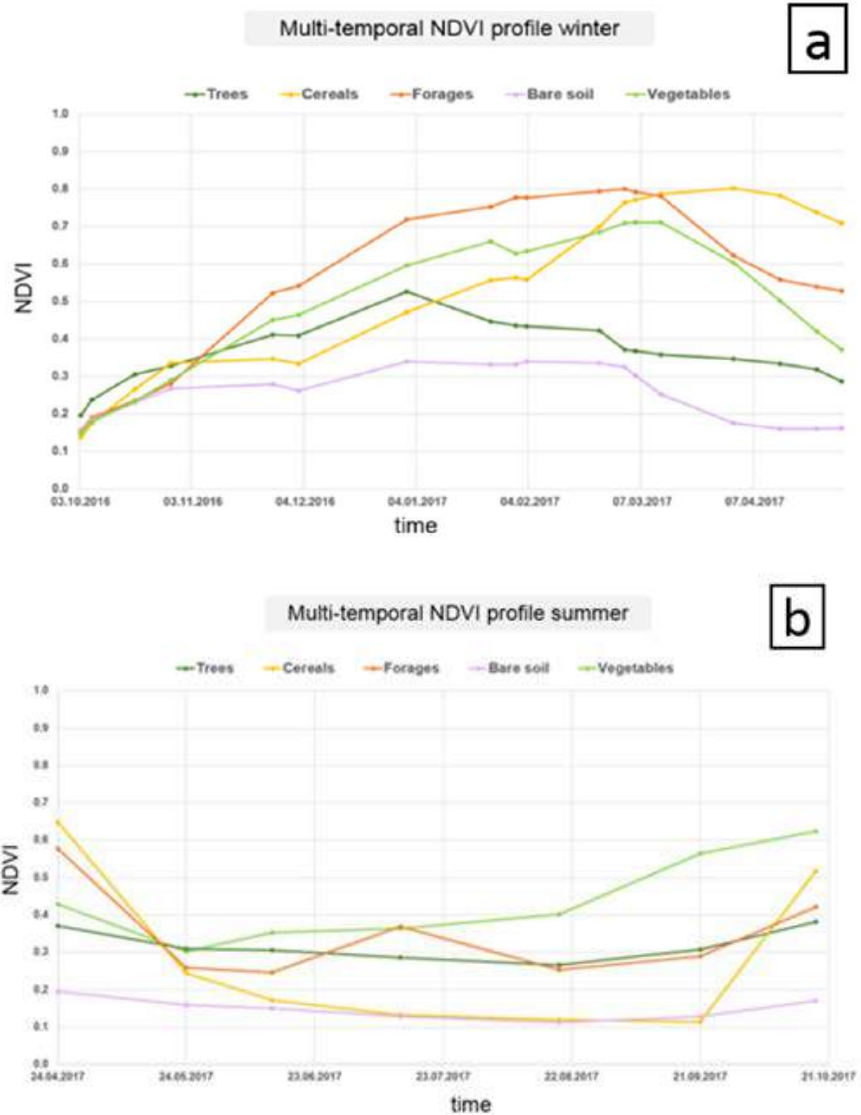


**Figure 11:** Multi-temporal NDVI profiles for a) winter 2016/2017 and b) summer 2017

The analysis of the profiles leads to the determination and creation of specific multi-temporal features that allow to better distinguish the different crop types from each other. In total, four multi-temporal features have been identified as useful for distinguishing the different crop types and are therefore retained for the later crop mapping: maximum NDVI, difference maximum-minimum NDVI, maximal slope and emergence date (EMD). Those features are represented schematically in Figure 12. More details can be found in (Dubois et al., 2018). Those additional features are then used for the land use classification, which aims the differentiation between major crop classes corresponding to different water needs.

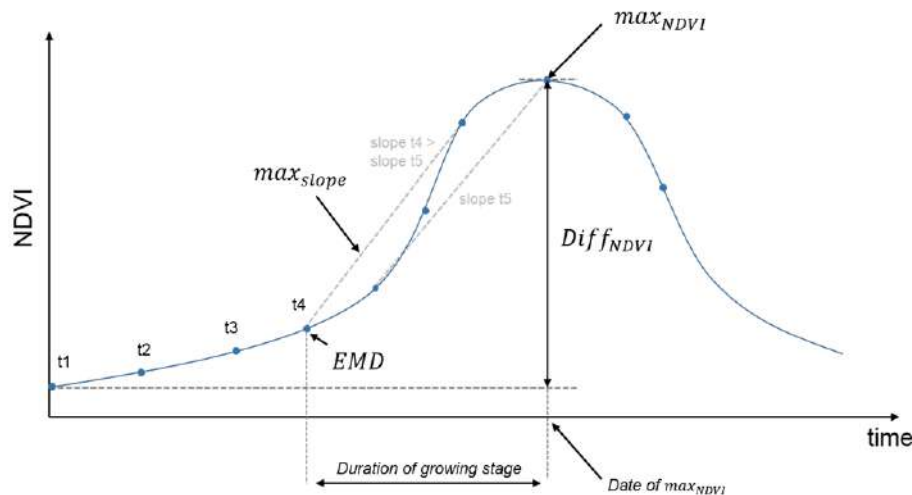


**Figure 12:** Schematic representation of the different multi-temporal features

Maximum Likelihood classification is applied for the macro-classes using all spectral bands of Sentinel 2 and the additional multi-temporal features. Relying upon the results of this classification, crop water requirement is estimated. For this purpose, a tool (excel sheet) based on the FAO method (Allen, 1998) has been set up. It aims at determining the crop evapotranspiration, which characterizes the water need of a specific crop by determining the amount of water used by the crop through evaporation and transpiration under ideal conditions. Using mainly climatological data and FAO standards, a reference evapotranspiration as well as specific crop coefficients are determined, leading to the calculation of the crop specific evapotranspiration. The results of the crop mapping are used for refining the calculation and adjust the FAO standard crop coefficient values to the local conditions. The macro-classes infer in the determination of the specific crop coefficient. The respective area of each macro-class serves as weighting factor for the calculation of the total volume of water needed for the entire agricultural area. Additionally to the crop evapotranspiration, the effective water need is determined for each month by subtracting the effective rainfall, which can be obtained by climatological data. A detailed explanation of the different formulas and intermediate results can be found in (Dubois et al., 2018).

### 3.2.3 Results

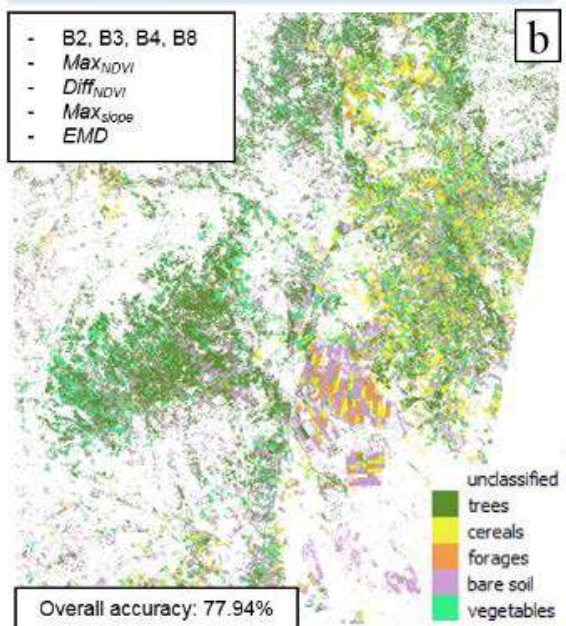
In this section, the results of the classification for the macro-classes as well as the estimation of the water needs are shown and discussed. The classification results (tile SNE) for the different agricultural seasons and classifier/ band combinations are presented in Figure 13.



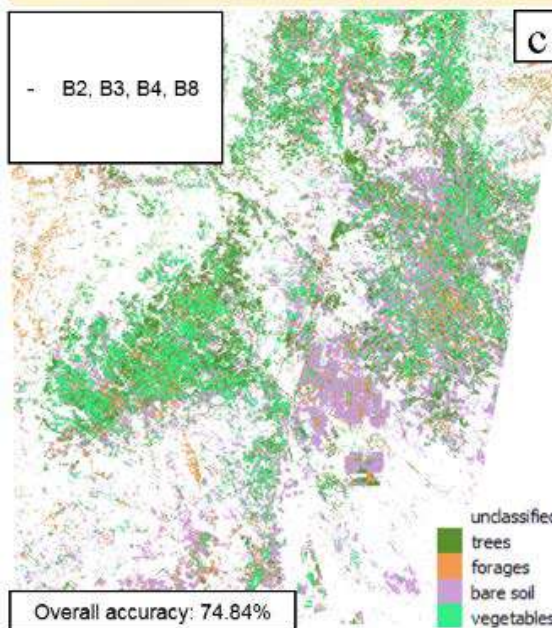
S2 RGB composite Winter (05.03.17)



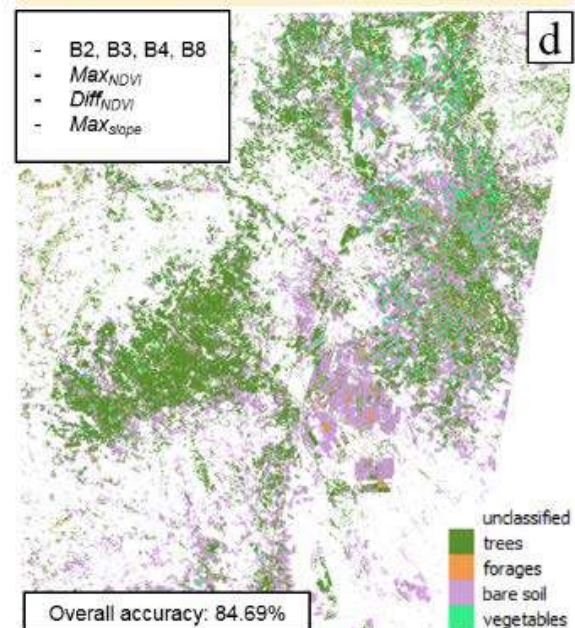
Winter – Maximum Likelihood



Summer – Maximum Likelihood



Summer – Maximum Likelihood





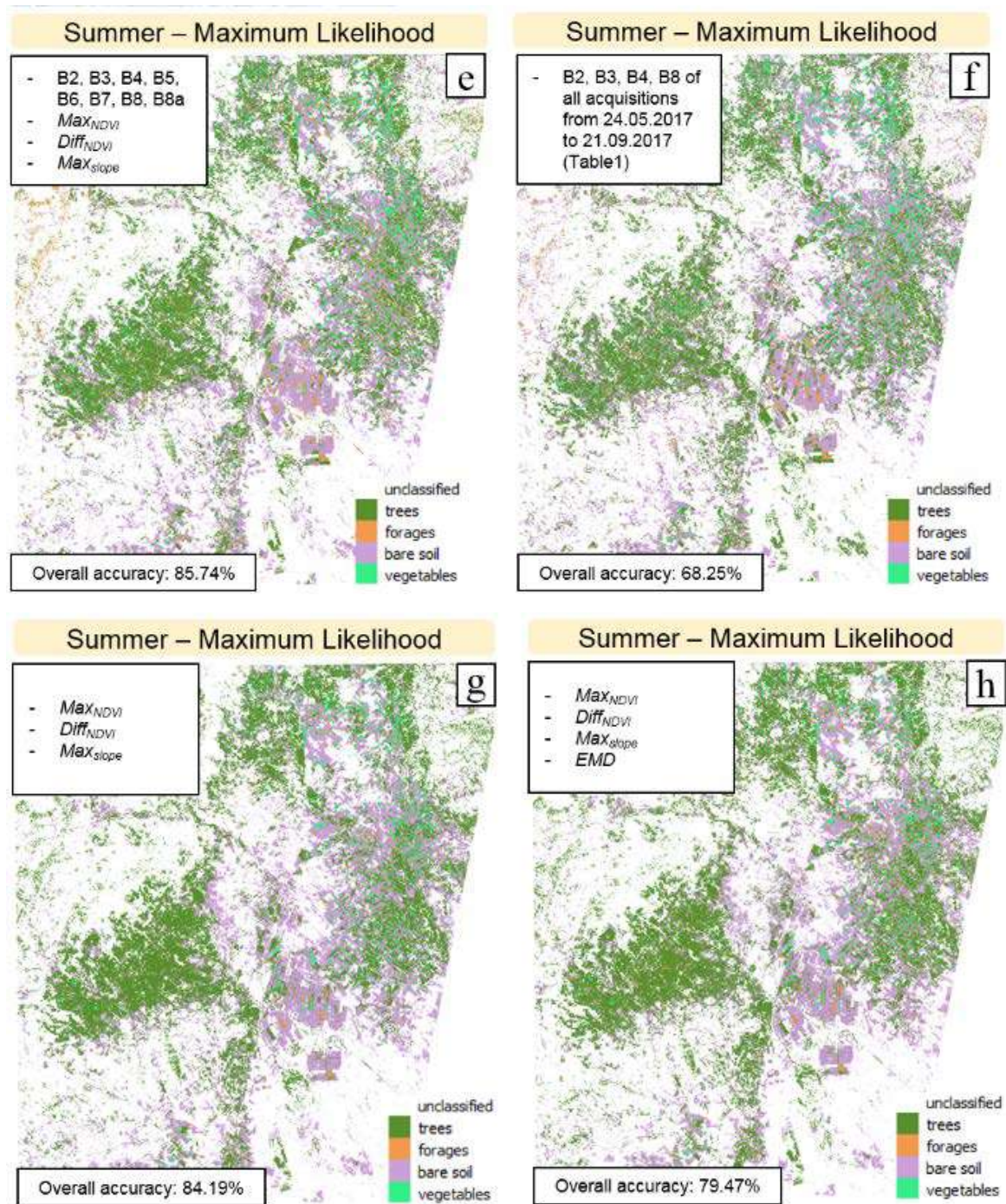


**Figure 13:** Classification results; classification performed for winter on the acquisition from 05.03.2017 and for summer on the acquisition from 19.08.2017, Sentinel 2 tile SNE, dates providing the best separability between the classes according to the NDVI profiles.

For the winter classification, five classes are considered. The classification is performed using Maximum Likelihood (ML) algorithm. A look at the confusion matrix, in order to analyse the quality of the differentiation between cereals and forages, shows a good producer's accuracy for the forages (67%). For the macro-class cereals, ML achieves a user's accuracy of 76%. A high producer's accuracy shows a high correctness of the classification whereas a high user's accuracy stands for a high reliability. This is important as it shows that forages and cereals can be well distinguished using the proposed approach, even if they are spectrally very similar.

This separation between forage and cereals is important, as their experience shows that forages and cereals need different amount of water.

For the summer classification, only four classes are considered, as cereals are not cultivated in summer and the fields are bare. Different band combinations and multi-temporal features are analysed. The best overall accuracy (85.74%) is achieved using 8 bands of Sentinel-2 (Figure 13e) and the multi-temporal features  $Max_{NDVI}$ ,  $Diff_{NDVI}$  and  $Max_{slope}$ . Using only the four principal bands (Figure 13d) and the same features, the overall accuracy is similar (84.69%). As using less bands permits a faster classification processing, the use of only four spectral bands is retained. In order to analyse the contribution of the multi-temporal features, different analyses are performed: the use of the four spectral bands only (Figure 13c) provides an accuracy of 74.84%, which is 10% less than using the spectral bands together with the multi-temporal features. Especially for the trees, the producer's and user's accuracies are in this case of about 37%, which is also visible in the classification results, as most of the tree plantations in the West have been classified as vegetables. The user's accuracy of vegetables is in this case only 18%. The use of the four spectral bands of all summer acquisitions (Figure 13f) instead of the multi-temporal features yields worse overall accuracy (68.25%). On the contrary, using only the multi-temporal features for classification (Figure 13g), leaving apart the spectral bands and the emergence date feature, yields a very good overall accuracy of 84.19%. Using additionally the temporal feature  $EMD$  (Figure 13h) slightly deteriorate the accuracy (79.47%). This can be explained as the emergence date may not always characterize a specific crop type, but depends principally on the sewing date, which depends on the farmer's practice. Therefore, the emergence date is a useful information for the authorities to know when a crop will need more water intake and for the subsequent determination of monthly crop specific coefficient, but should be used only as an additional information to the crop type classification, and not directly for the classification. A closer look at the confusion matrix of the two best classification results reveals a very good classification of forages and bare soil. Also the producer's accuracies of trees and vegetables are very high (around 90%). The user's accuracy of vegetables is around 60% and the user accuracy of trees around 50%, meaning that in summer, only 50% of the classified trees are really trees. As for the winter, the user's accuracy of the trees is around 80% and tree plantations do not change from year to year, it is preferable to use the tree mask extracted during the winter classification, as it is more reliable.

The confusion matrices with the corresponding producer's and user's accuracy are given in Appendix 1.

Based on the classification results, water needs for a specific month or a specific season are calculated. Using the developed tool in combination with free available climatological data, a total water volume of 20 Mm<sup>3</sup> has been estimated for the month of March 2017 for the considered area. No direct validation is possible for 2017. However, the water consumption of specific zones within this area is known by the water authorities for the winter season 2015-2016. Even if the cultures were probably not exactly the same as for the winter season 2016-2017, we compared the water consumption of one of those zones in March 2016 with the estimated water need for March 2017, in order to validate the order of magnitude. For this zone with a surface of 478ha, the reference of March 2016 indicates a water consumption of 120,919 m<sup>3</sup>. For the same area in March 2017, the calculation yields 149,186 m<sup>3</sup>, which is in the same order of magnitude. This result is very encouraging, especially as the amount of water indicated in March 2016 corresponds to the volume of water which has been charged by the water



providers, and may be slightly underestimated compared to the real consumption due to the potential presence of non listed boreholes.

Using the classification results (tile SNE), a map of the emergence date characterizing the time of year where the crops start to need water (Figure 14a), and a map of the water need for March 2017 (Figure 14c), derived from the month specific crop evapotranspiration (Figure 14b) are presented.

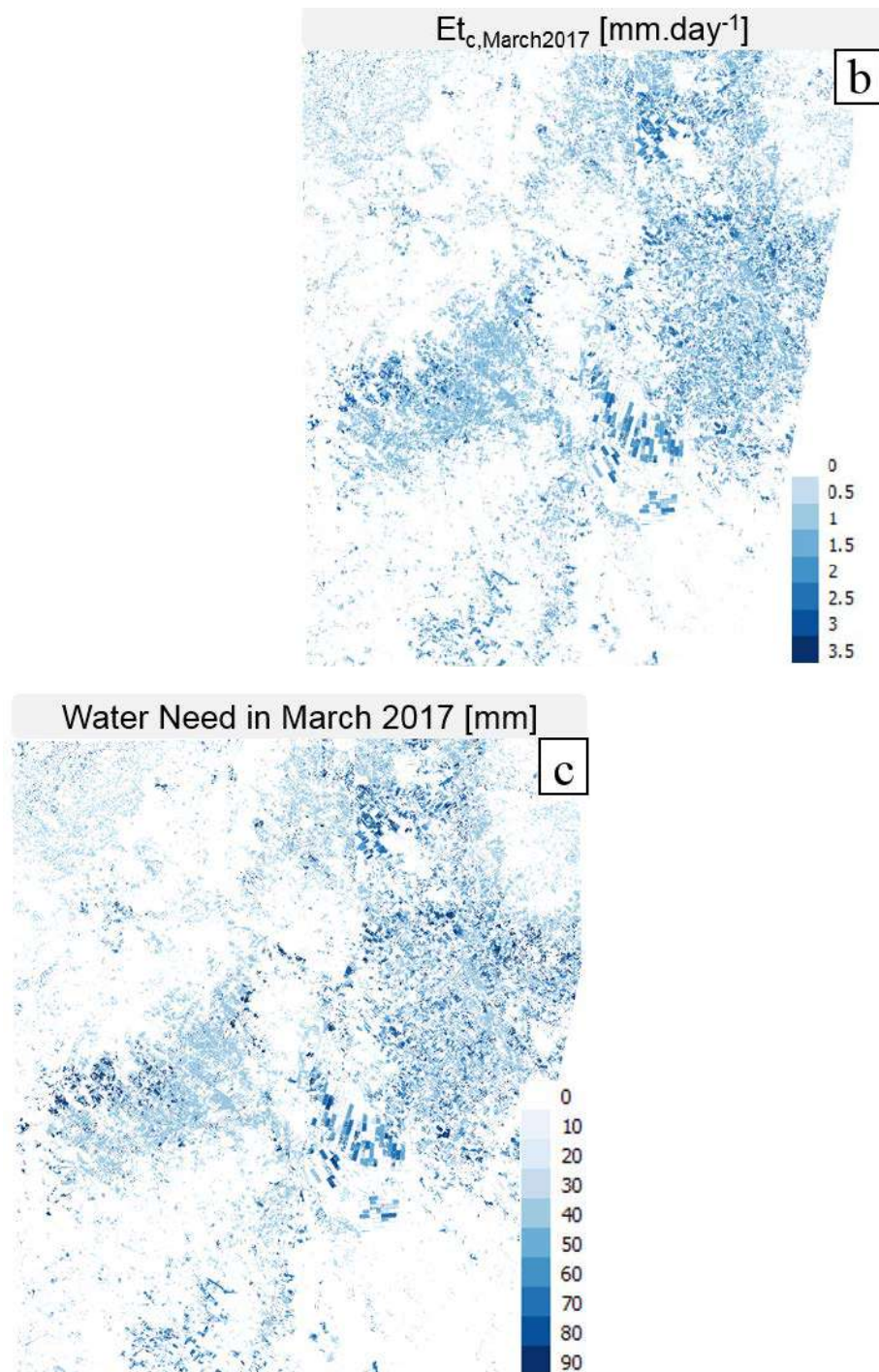


**Figure 14:** a) Map of the emergence date winter 2016/2017 and b), c) water need maps for March 2017, Sentinel 2 tile SNE

### 3.3 RADAR Processing

#### 3.3.1 Data

For Tunisia, current satellite missions (commercial TerraSAR-X and open source Copernicus Sentinel 1 data), as well as archive data (open source Envisat ASAR data) have been investigated. Table 4 resumes the number of available acquisitions for each dataset. A detailed overview of the acquired datasets and acquisition dates is given in Appendix 2.

**Table 4:** Number of available acquisitions and time span for each considered sensor

	Ascending	Descending
Envisat ASAR	-	22 datasets, from 09.2003 to 09.2010
TerraSAR-X	15 datasets, from 12.2015 to 06.2016	-
Sentinel 1	91 datasets, from 03.2015 to 07.2017	86 datasets, from 02.2015 to 07.2017

The number of available data for Envisat ASAR and for TerraSAR-X is low for ground motion analysis. Yet, as the time span between the TerraSAR-X acquisitions is only 11 days, the detection of coherent scatterers, even over the limited period, is possible and a robust ground motion estimation was achieved. The number of available acquisitions with Envisat ASAR is slightly higher, yet for a period of several years. The average time interval between acquisitions is very large (from 1 month to more than 2 years). The later involving that coherent scatterers for ground motion analysis cannot be detected robustly.

The number of acquisitions available with Sentinel 1 is higher, the acquisition rate increasing by a factor of two (from every 12 days to every 6 days) in October 2016. Sentinel 1 data are available in both directions of acquisitions, allowing a comparison and complementarity of the estimated ground motion from both directions. Furthermore, with this ascending/descending configuration, a calculation of the real vertical motion as well as of the east-west motion component of the area is possible.

The ground coverage differs for each sensor (Figures 15-19). For TerraSAR-X and Envisat ASAR, the whole scene was considered for processing. For TerraSAR-X because of the necessary area coverage in order to encompass the whole motion process, for Envisat because of the much lower data size which allows a fast processing even with whole scenes. For Sentinel 1, only the swaths and burst covering the area of interest have been used, in order to reduce the computing time.

#### 3.3.2 Methodology

The determination of the ground motion was performed using both RADAR interferometric methods PSI (Persistent Scatterer Interferometry) and SBAS (Small Baseline Subset). PSI aims at the detection of long time coherent point targets (Persistent Scatterers, PS), usually created by strong corner reflectors of man-made objects, showing very stable reflectivity values over time. PSI is thus suitable for the analysis of urban areas. SBAS aims at the detection of distributed scatterers (DS), whose added reflection is coherent over time. SBAS is more suited for the analysis of rural areas, where PS targets are rare but DS targets exist. Therefore, SBAS was used for all datasets, as it allows an area-wide analysis, not bound to urban areas. PSI has been applied for completeness, in order to show the density of point targets in the results compared to SBAS. Table 5 resumes which data were processed with which methods. In total, five calculations have been performed.

**Table 5:** Method used for the processing of the different data

	PSI	SBAS
Envisat ASAR	-	whole dataset (see Appendix 2)
TerraSAR-X	-	whole dataset (see Appendix 2)
Sentinel 1	From 02.07.2015 to 14.06.2016, ascending	whole dataset ascending (see Appendix 2) whole dataset descending (see Appendix 2)

As it was possible with Sentinel 1 to estimate the ground motion in both directions of acquisitions, the real vertical motion-as well as the east-west motion-have been derived, using the respective geometries. Due to the orbit constellation of the satellites, an estimation of the motion in north-south direction is not possible.

### 3.3.3 Results

Table 6 resumes for each dataset the principal processing parameters. Processing parameters have been used depending on the data quality and considered time periods. The different ground motion maps corresponding to Table 6 are presented in the Figures 15 to 19.

**Table 6:** Principal processing parameters for the different datasets

	Envisat ASAR	TerraSAR-X	S1-PSI	S1-SBAS asc.	S1-SBAS desc.
Max Normal Baseline	75%	30%	-	30%	30%
Max Temporal Baseline	730d	40d	-	60d	60d
Allow disconnected blocs	True	False	-	True	True
DEM	SRTM-3 V4	SRTM-3 V4	SRTM-3 V4	TDM	TDM
Number of GCPs	213	25	1 per 25km <sup>2</sup>	85	84 (same as for Asc.)
3D Unwrapping	False	True	-	False	False
Decomposition Level	2	1	-	1	1
Atmospheric high-pass Filter	365d	365d	365d	365d	365d
Atmospheric low-pass filter	1200m	2000m	2000m	2000m	2000m
Product Coherence Threshold	0.1	0.4	0.75	0.35	0.35
Max/Min Velocity	-	-	+/-25mm	-	-
Number of effective scenes	14	14	27	89	77
Number of effective interferograms	25	27	26	247	250

The different appearances between PSI and SBAS is due to the fact that the result of the PSI analysis is a vector file, whereas the result of the SBAS processing is a raster. It is possible to convert the raster in vector, however the required time and the resulting data size is not suitable for further analysis. Therefore, the original (default) data format was used.



### PSI on Sentinel 1 data

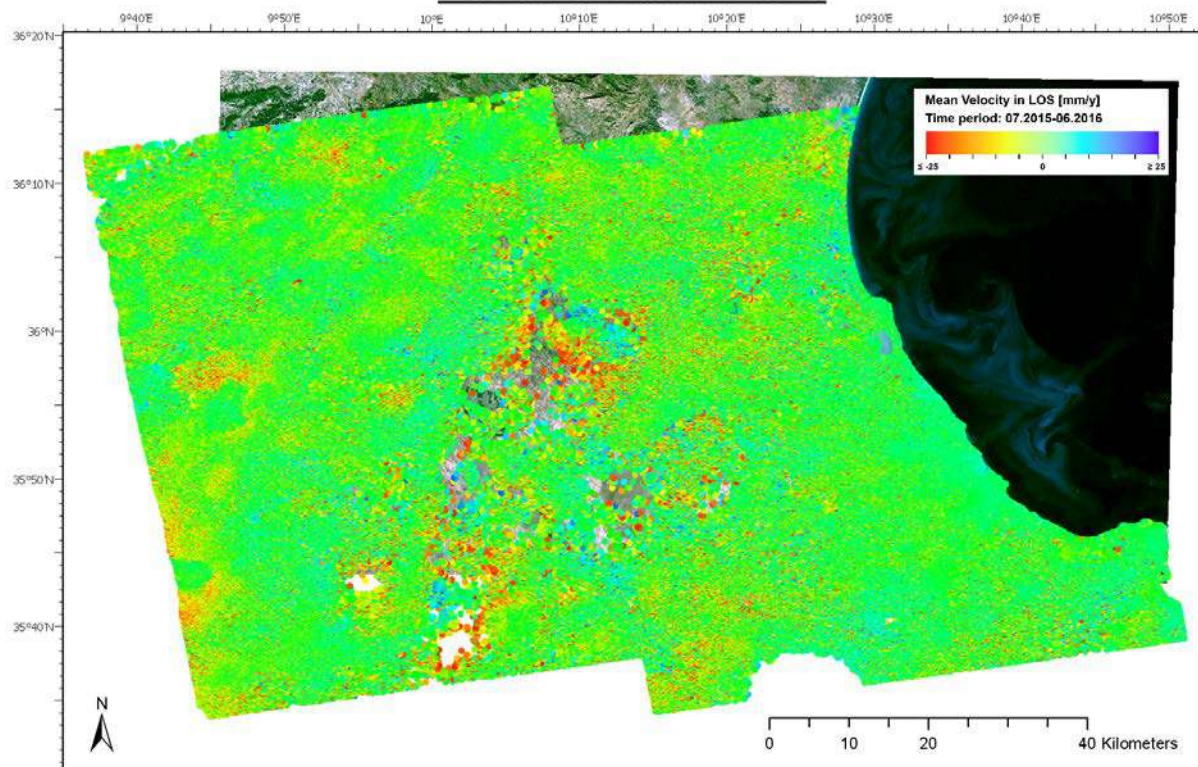


**Figure 15:** Ground motion map for PSI on Sentinel 1 data

### SBAS on TerraSAR-X data

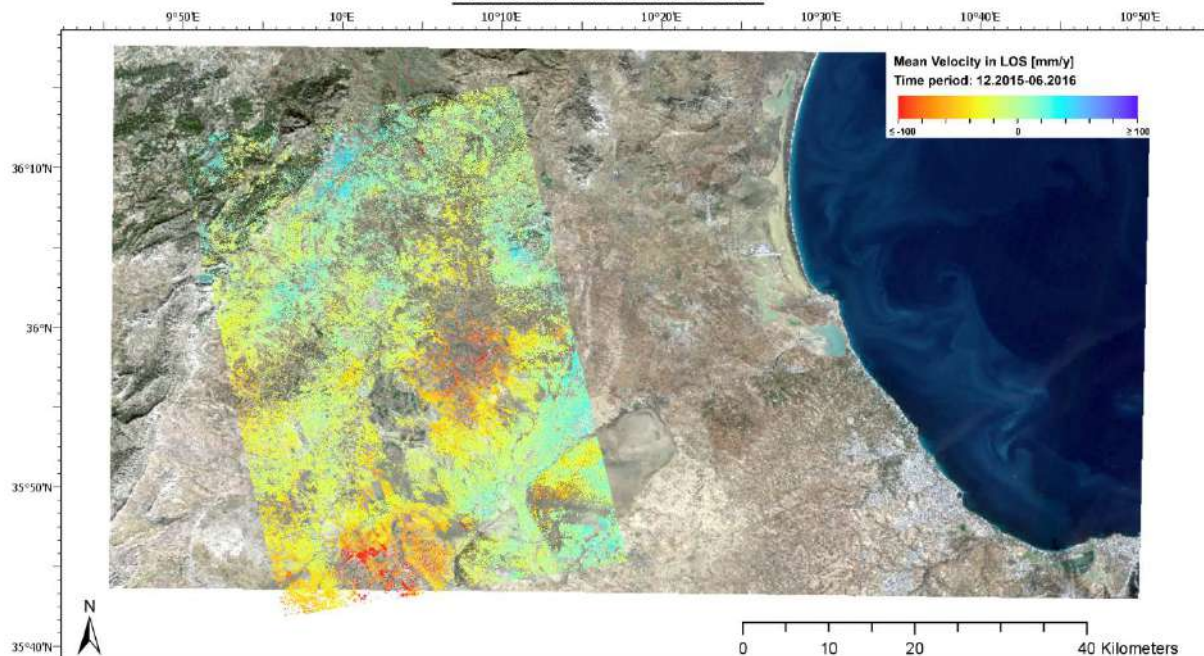


**Figure 16:** Ground motion map for SBAS on TerraSAR-X data

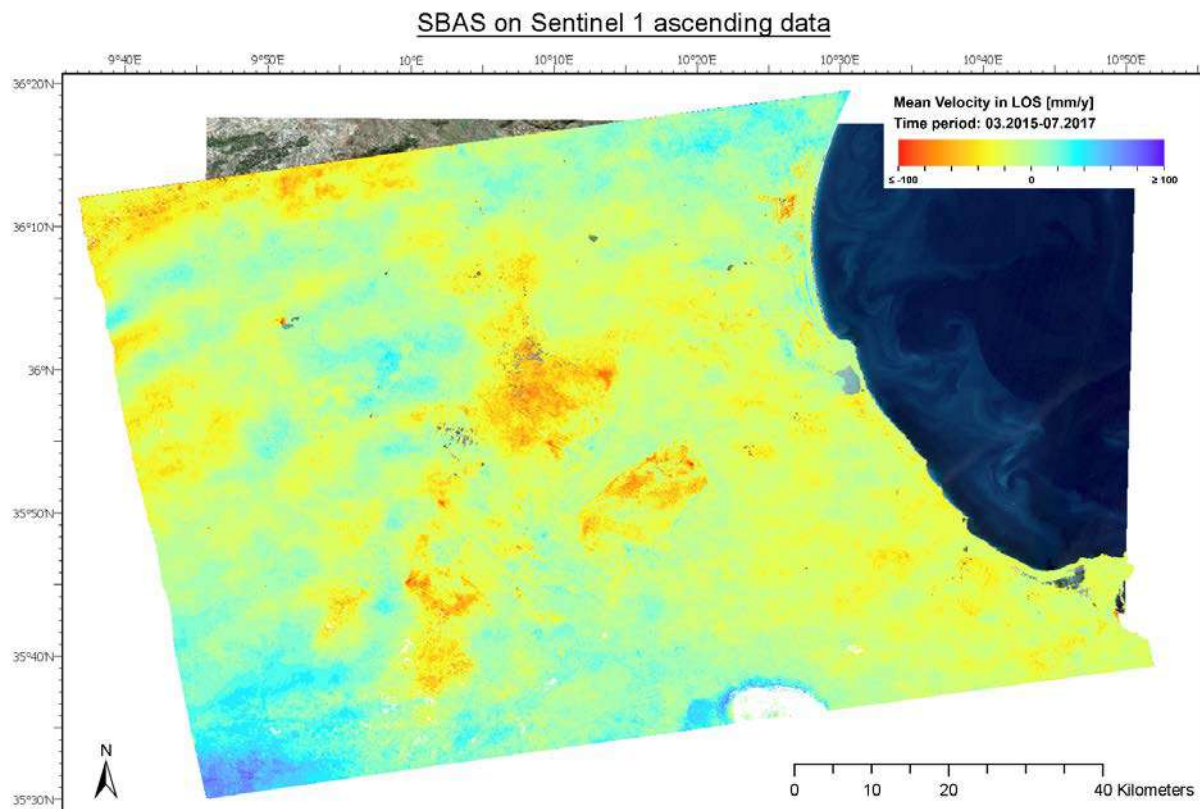


**Figure 17:** Ground motion map for SBAS on Sentinel 1 ascending data

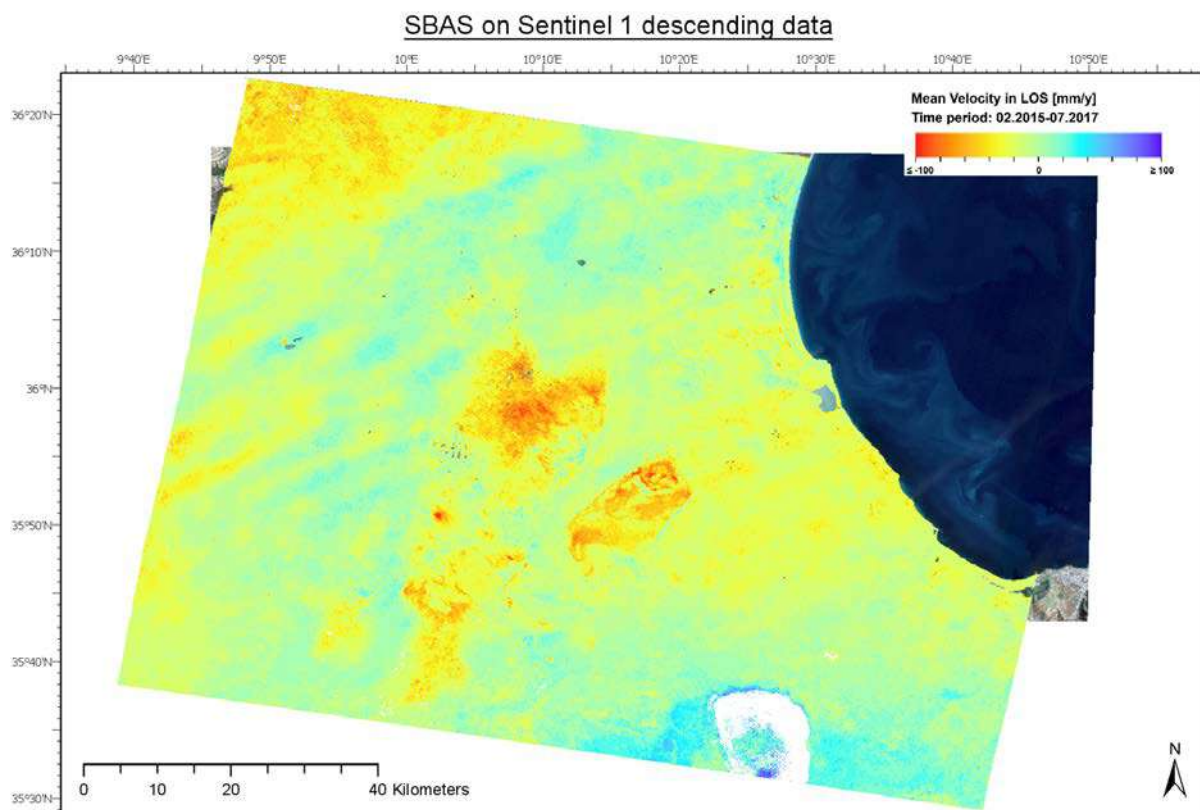


**Figure 18:** Ground motion map for SBAS on Sentinel 1 descending data



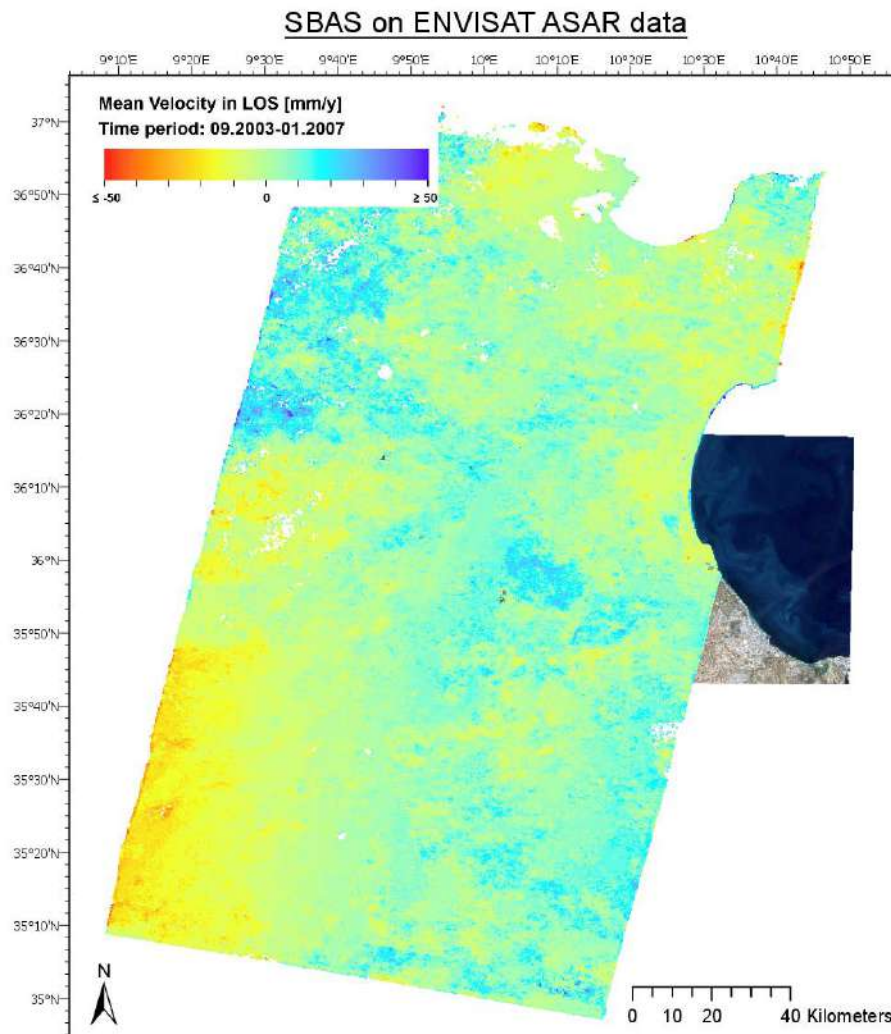


**Figure 19:** Ground motion map for SBAS on ENVISAT ASAR data

### Comparison between PSI and SBAS results

At a first glance, the PSI and SBAS results show similar deformation patterns (Figures 15-19).

A direct comparison of the PSI and SBAS results is not possible yet, as

- Different periods of time, thus neither the same time span nor the same number of acquisitions were considered for the processing
- Different parameters were used for the processing

However, a short analysis of the single results as well as a short comparison in terms of PS density and velocity values is given here.

It is obvious from Figure 20a and b that the PS density in rural areas and in particular in the area of interest is insufficient, compared to the DS density obtained with the SBAS methodology. It is also because of the chosen coherence threshold for PSI, which is much higher than the one chosen for SBAS, therefore retaining less scatterers for PSI as for SBAS.

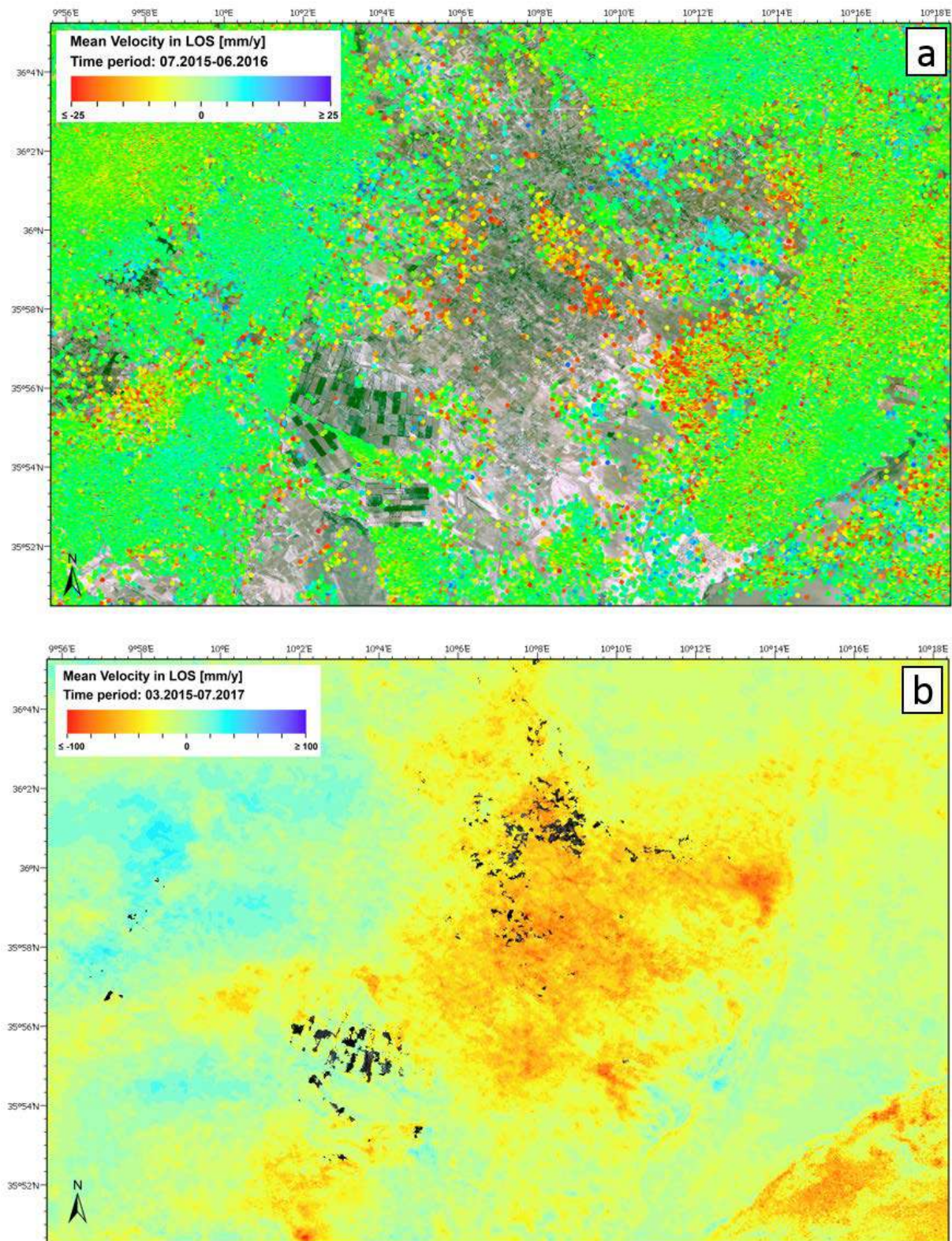


**Figure 20:** a) Velocity map from PSI processing for the region of Nebhana; b) Velocity map from SBAS processing for the region of Nebhana;

The PS result over the agricultural region of Nebhana (Figure 20a) shows areas of subsidences in the center, in the far north east and in the south-west hills. These locations correlate with the areas of subsidences observed in the SBAS result. An area of uplift is



observable too, in the north east of the agricultural zone. However, in the SBAS result, this area in the north is characterized by a more moderate subsidence rate up to a stable zone.

A further remark concerning the PSI analysis is that the results show more noise than by SBAS. This is partly because the SBAS processing performs an additional spatial filtering, but also because more scenes were used for SBAS processing, yielding a smoother result. Finally, the maximum displacement range was set for the PSI processing at  $\pm 25\text{mm/a}$ , which is low compared to the velocity observed in the SBAS results. A recommendation would be here to reprocess the PSI analysis by setting a larger range of displacement velocities (for example  $\pm 100\text{mm/a}$ ).

#### Comparison between archive and current data

A visual comparison of the SBAS result between archive Envisat ASAR data and current Sentinel 1 data show opposite deformation patterns between both time periods (Figure 21). The coherence threshold of the Sentinel 1 data was set at 0.35, in order to have enough spatial information in rural areas. The coherence threshold chosen for the archive data is even lower (0.1). This was necessary as the archive data show very high temporal decorrelation because of the larger time span between available acquisitions. The low product coherence threshold implies a very careful analysis of the results, as an important noise component may remain in the observed deformation patterns. An important noise may induce unwrapping problems of the interferometric phase, yielding to noisy or aberrant deformation patterns, instead of smoothed spatial appearance. This is well observable for both SBAS results, where the apparent deformation pattern is not smooth. At this point, it is also important to mention the very different number of images and the timespan between the SAR scenes used for SBAS processing (see Appendix 2): for the ENVISAT processing, only the scenes marked in grey in Appendix 2 have been used in the final processing in order to consider only more coherent interferograms. Those represent in total 14 scenes only instead of 86 scenes with Sentinel 1 data. Usually, a minimum of 20 scenes is required for such interferometric stacking techniques.



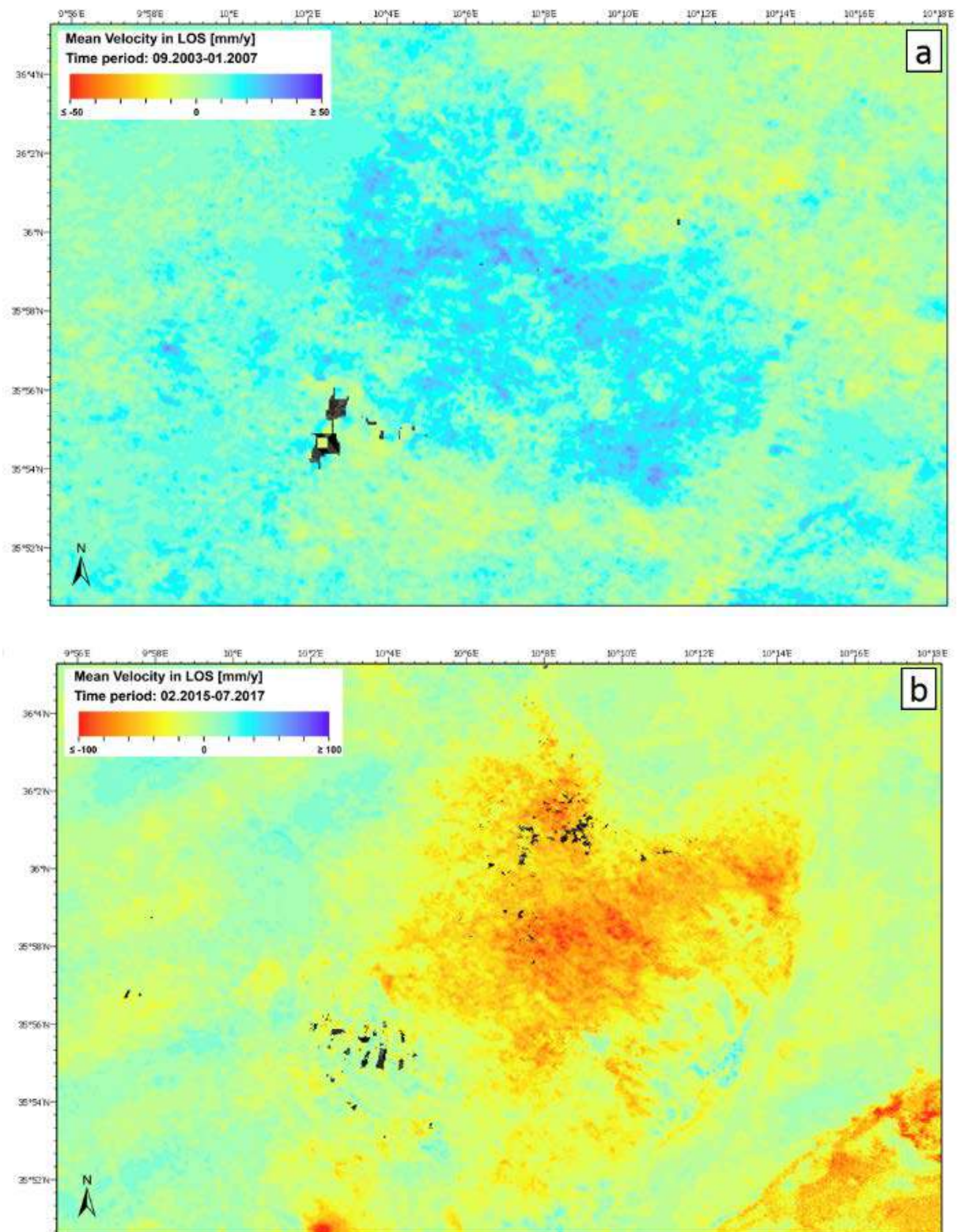


**Figure 21:** a) Velocity map from Envisat ASAR SBAS processing for the region of Nebhana; b) Velocity map from Sentinel 1 SBAS processing for the region of Nebhana; both processing are performed with descending datasets.

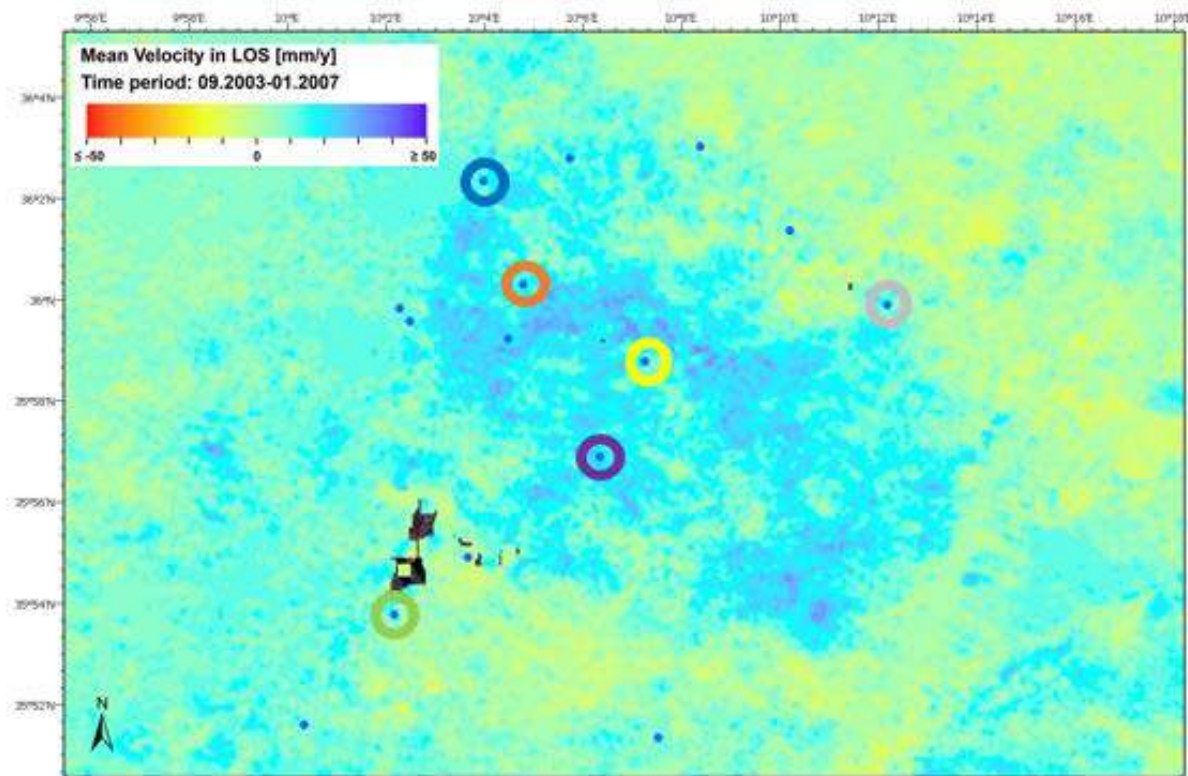
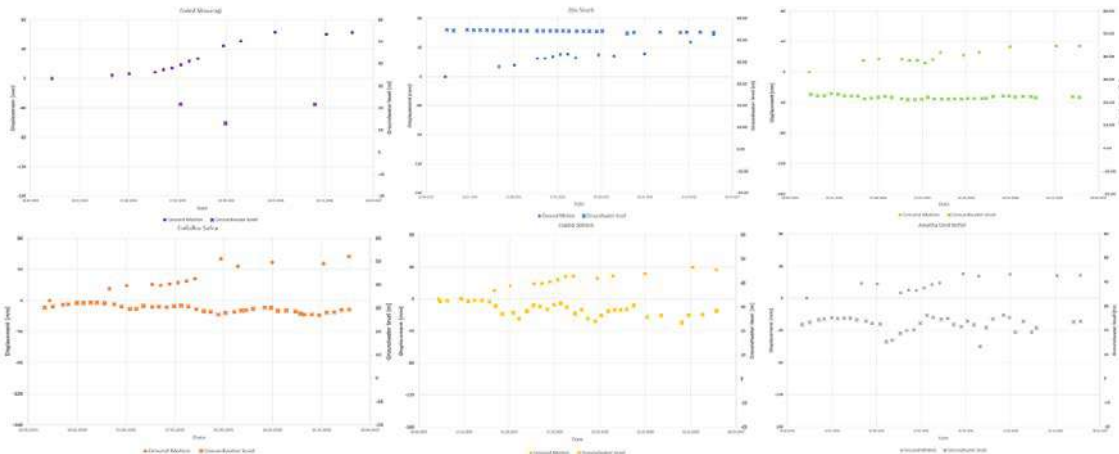


**Figure 22:** Velocity map from Envisat ASAR SBAS processing for the region of Nebhana and superimposed piezometer locations. The piezometers selected for further interpretation are encircled in color

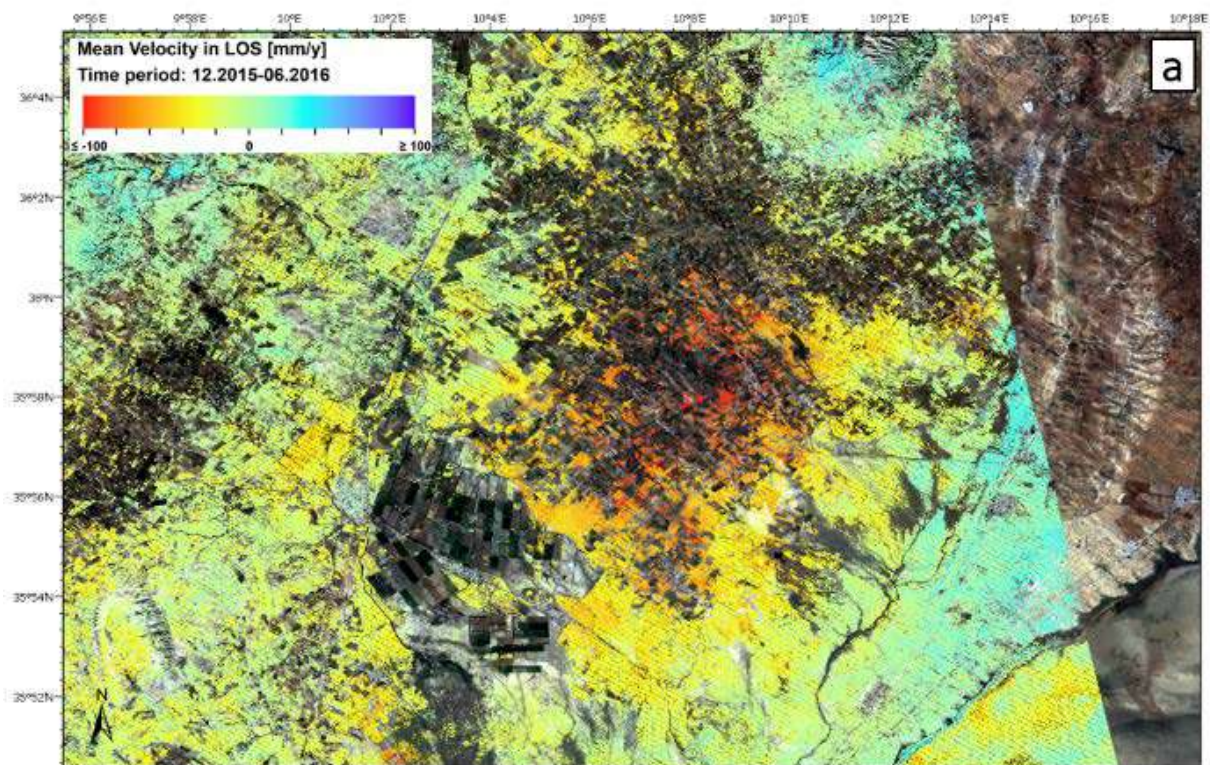
A closer analysis of the specific deformation patterns has been performed using available information about ground water level. Figure 22 shows the position of different piezometers in the Nebhana region and Figure 23 shows color-coded their respective ground water level's evolution compared to the corresponding displacement values from the SBAS processing, for the period of acquisition of Envisat ASAR data. The scales are chosen for the sake of better comparison with the Sentinel 1 analysis of Figure 20. A first comparison with Figure 20 shows both for ground water level and displacement a much steadier trend during the period 2003-2007 as during the period 2015-2017, indicating a strong decrease of the ground water level towards the recent years and a relatively slow motion in the last decade. The considered period of time for ENVISAT ASAR is twice as long as for Sentinel 1, but in this period, very small variations of the ground water level as well as very small ground motion rates are observed compared to those observed within the two years of Sentinel 1 acquisitions. At first glance, a correlation between ground water levels and ground motion is not observable for the ENVISAT ASAR data. The displacements observed with RADAR processing show a small uplift over the time period 2003-2007, whereas the ground water levels are stable over the whole time, showing seasonal effects of recharge and discharge. Due to the very low amount of RADAR data available for processing (14 scenes), the displacement results are not robust enough to make any reliable assumption. However, considering in Figure 23 Ouled Slimen (yellow) and Aouitha Oled Neffat (grey), some similarities in the behavior of the two curves could be interpreted. Both Ouled Slimen and Aouitha Oled Neffat show important ground water discharge - during summer 2005 and summer 2004, respectively - followed by a recharge. Even if there exists for those periods an important RADAR data gap, a similar trend can be interpreted in the displacement values, showing a negative displacement (subsidence)



followed by a positive displacement (uplift) for the respective periods and respective piezometers.



**Figure 23:** Ground water level (x) and corresponding displacement (•) at the different selected piezometers locations



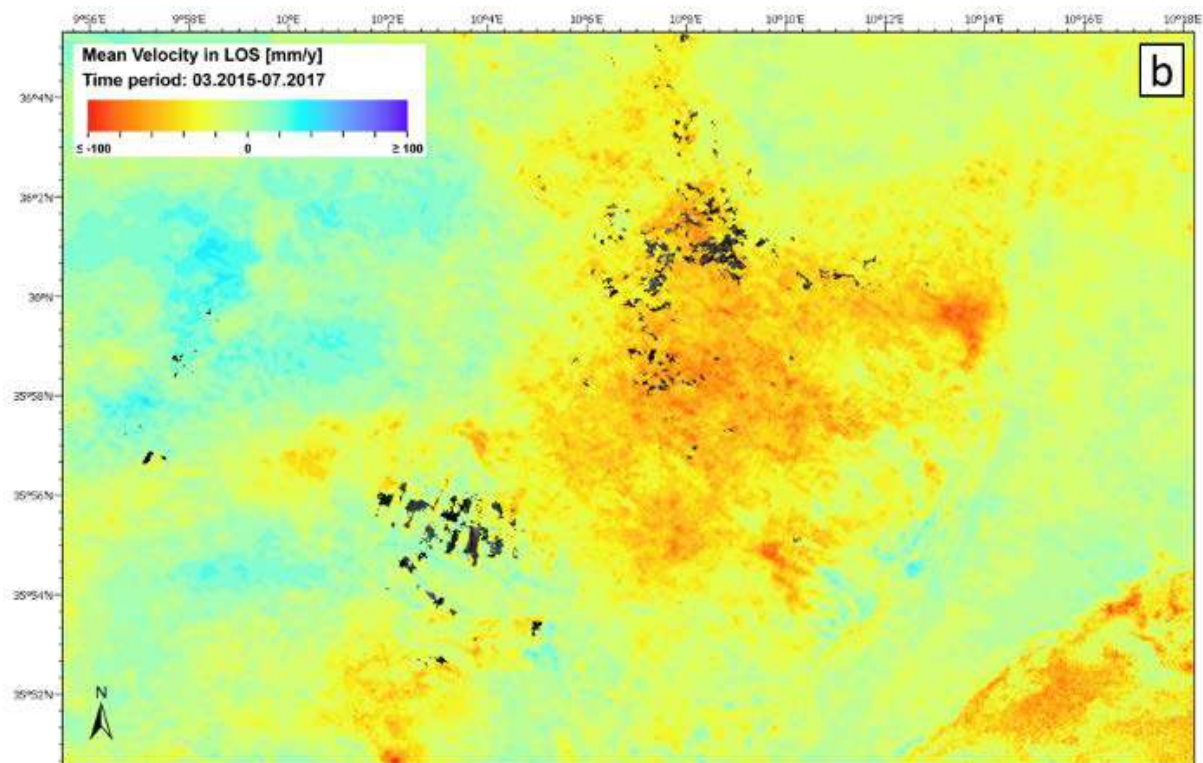


**Figure 24:** a) Velocity map from TerraSAR-X SBAS processing for the region of Nebhana; b) Velocity map from Sentinel 1 SBAS processing for the region of Nebhana; both processings are performed with ascending datasets.

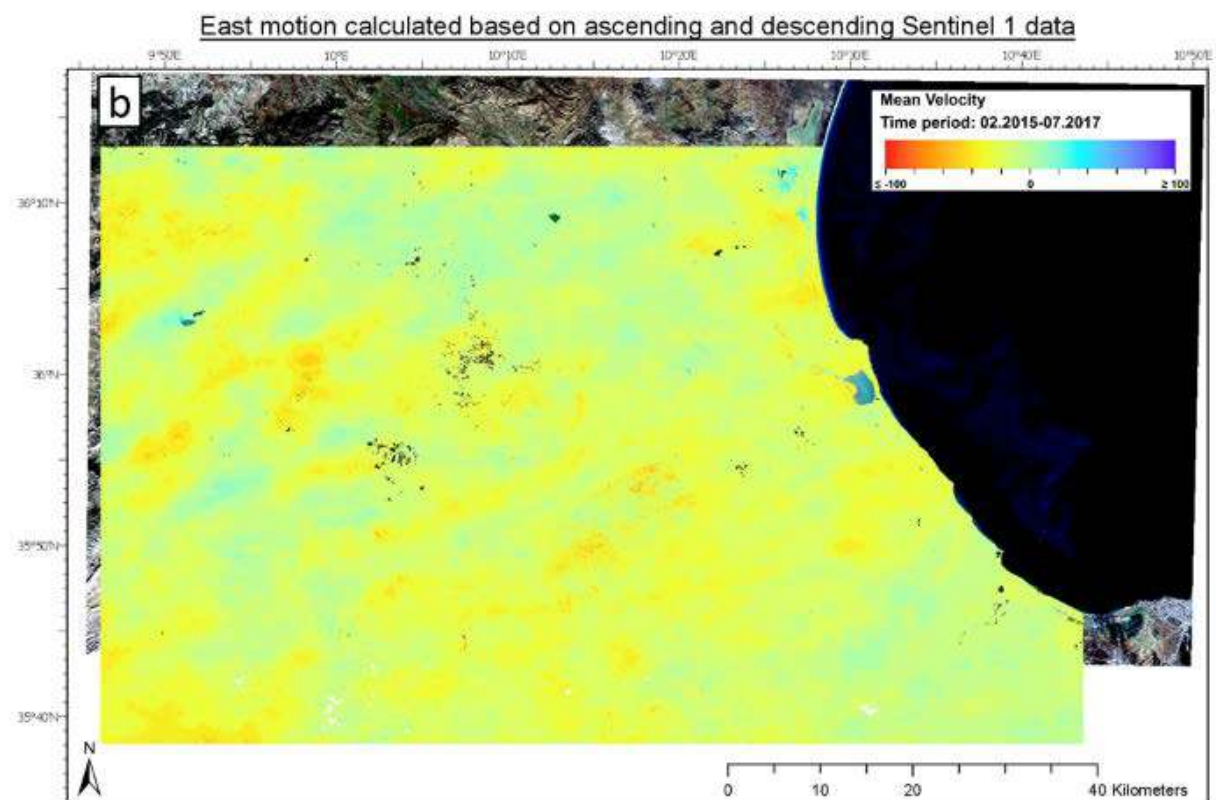
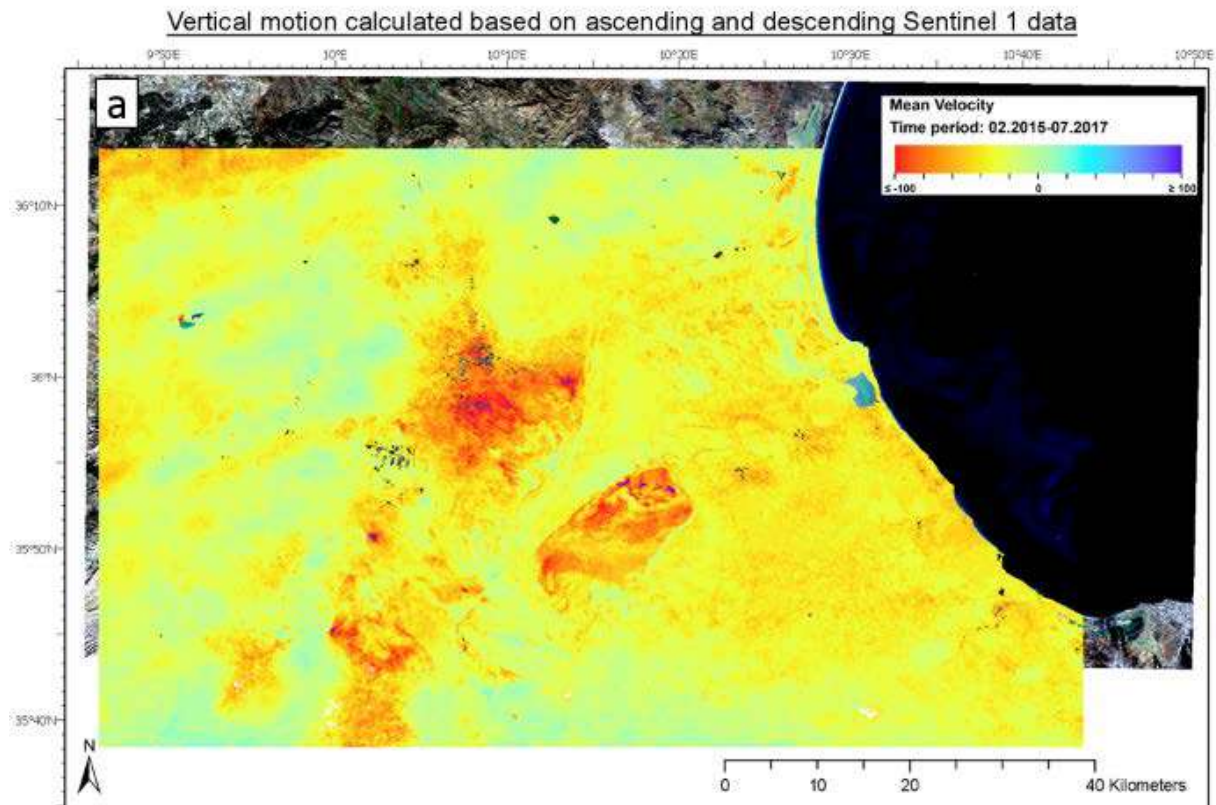
The influence of the coherence threshold is well observable in Figure 24 that shows the result of SBAS processing for TerraSAR-X data (Figure 24a) with a coherence threshold of 0.4 and the result of SBAS processing for Sentinel-1 data (Figure 24b) with a coherence threshold of 0.35. The higher the coherence threshold, the less scatterers are retained. As the area of interest is an agricultural area changing over time depending on the different crops, it suffers a high temporal decorrelation, explaining the low coherence threshold necessary to obtain deformation information in this area.

#### Interpretation of the velocities

For the interpretation of the ground motion, the SBAS results from both orbit directions have been fused in order to produce maps of the ground motion in vertical and in east-west direction (Figure 25). As expected on a flat area as the Nebhana plain, the main velocity component is in vertical direction, with velocities up to  $\geq 100\text{mm/yr}$ . The eastward velocity component shows no remarkable motion, the apparent westwards motion stripes being mainly due to remaining atmospheric artefacts. The following interpretation is therefore based on the vertical motion component (Figure 25a).

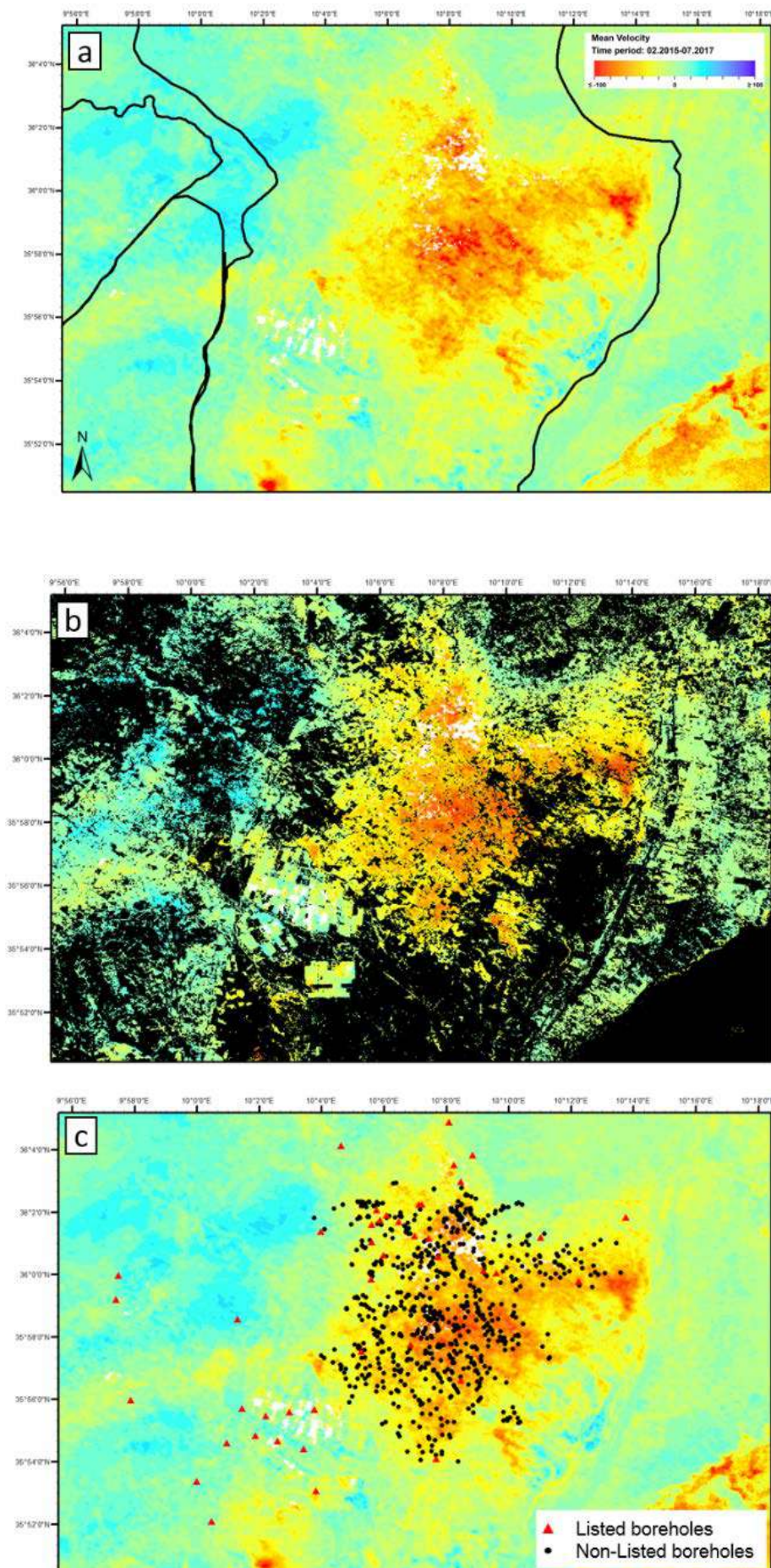
Considering the vertical motion, the apparent velocity pattern shows an important subsidence over the agricultural areas, up to  $-100\text{mm/yr}$ . The extent of the subsidence shows a spatial correlation with the location of the underlying aquifer, especially on the east border of the aquifer (continuous black lines in Figure 25a). Another spatial correlation can be found when combining the velocity map with a land use map. Figure 25b shows the velocity map superimposed with the cropland mask of the ESA CCI LAND COVER - S2 PROTOTYPE LAND COVER 20M MAP OF AFRICA 2016.



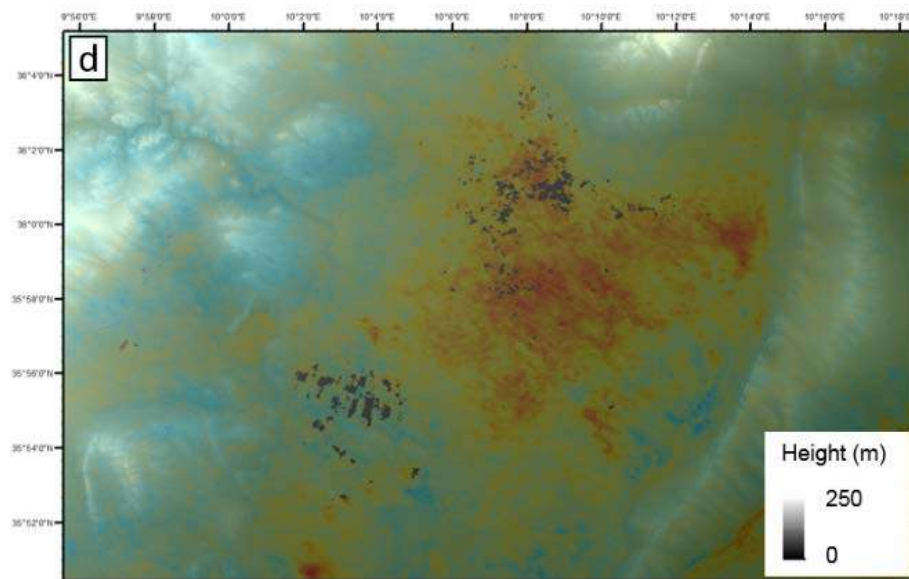


**Figure 25:** a) Vertical velocity from Sentinel 1 SBAS processing; b) Eastward velocity from Sentinel 1 SBAS processing



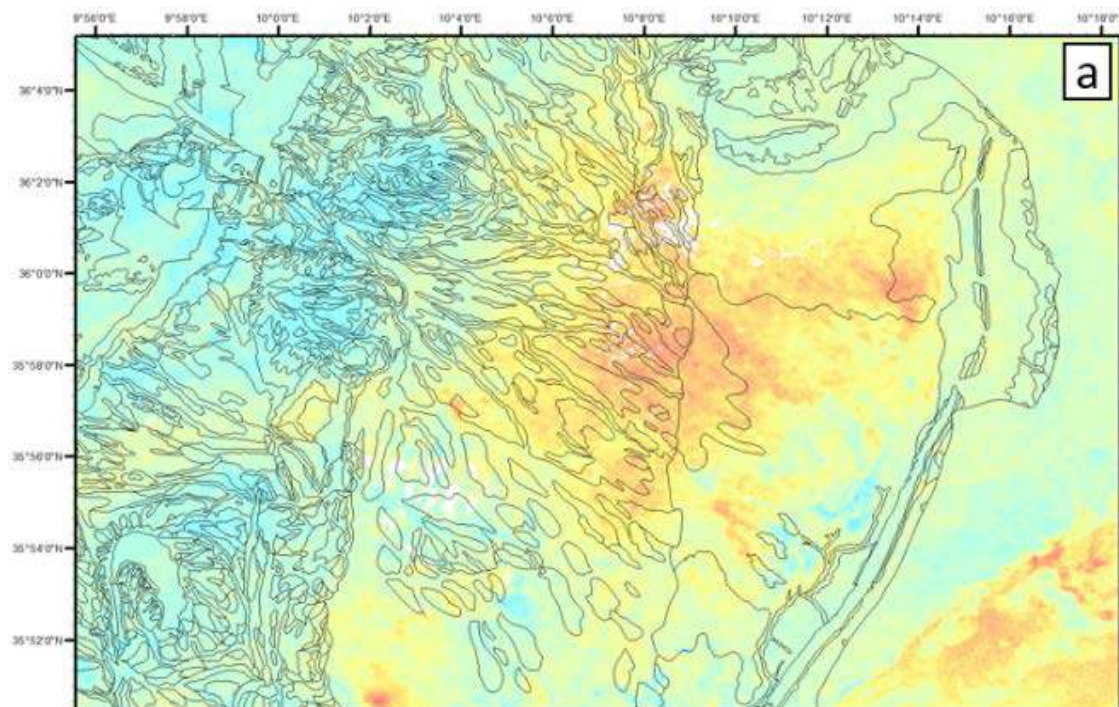


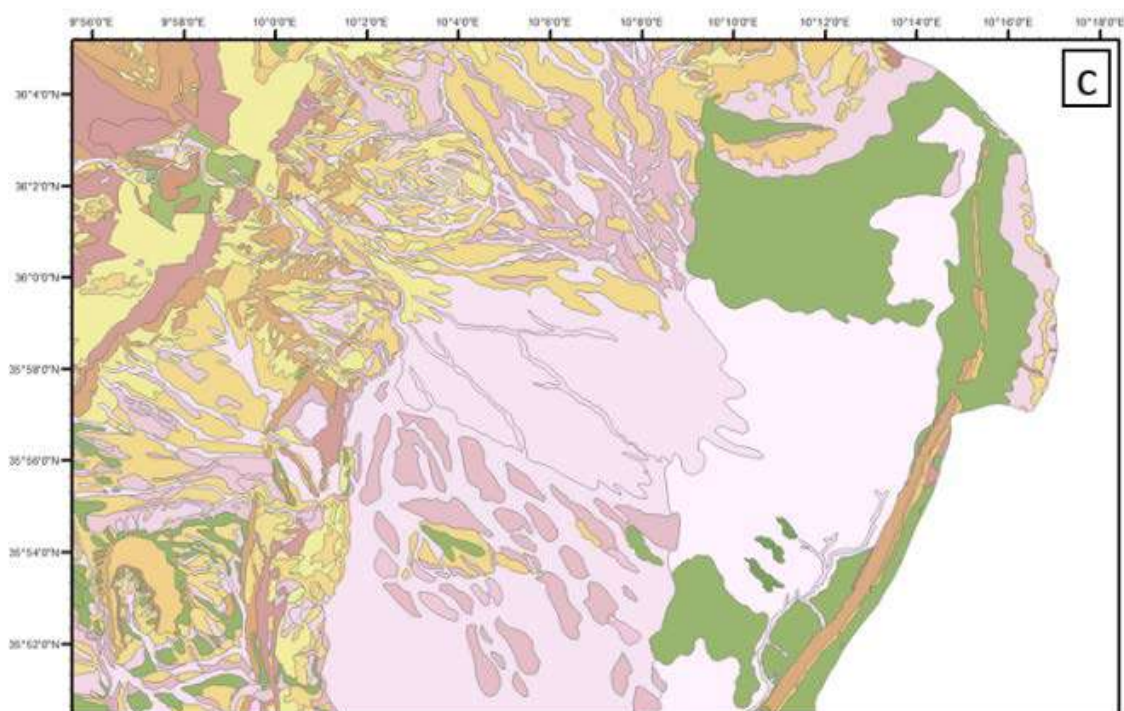
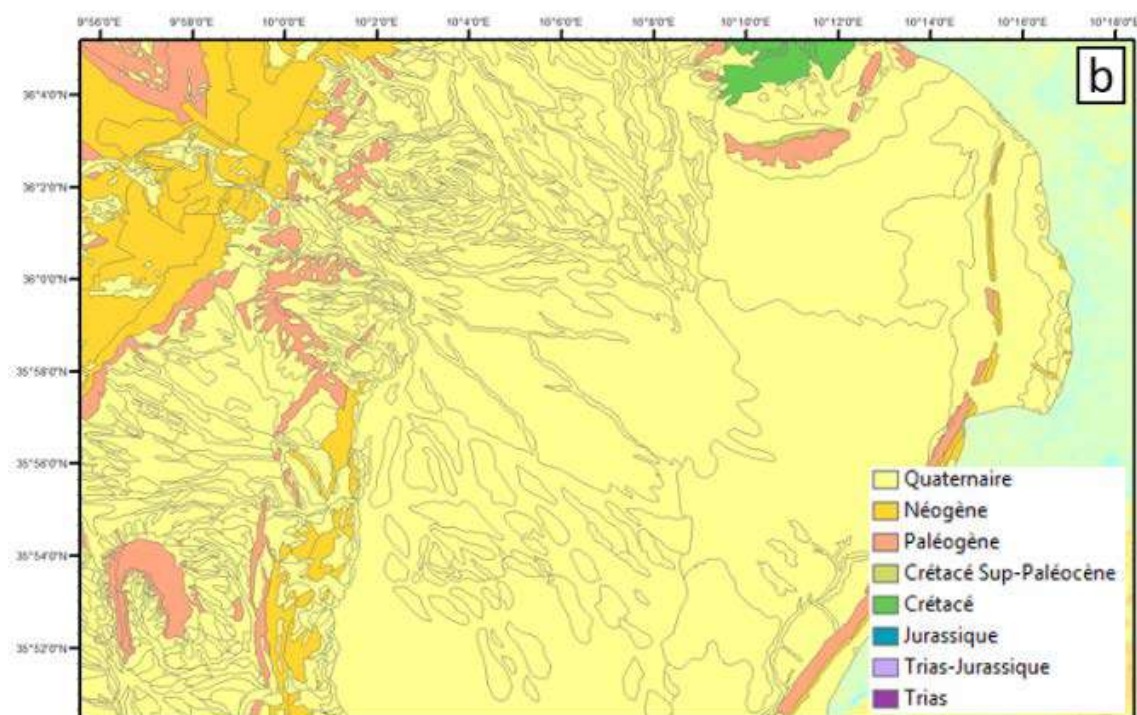




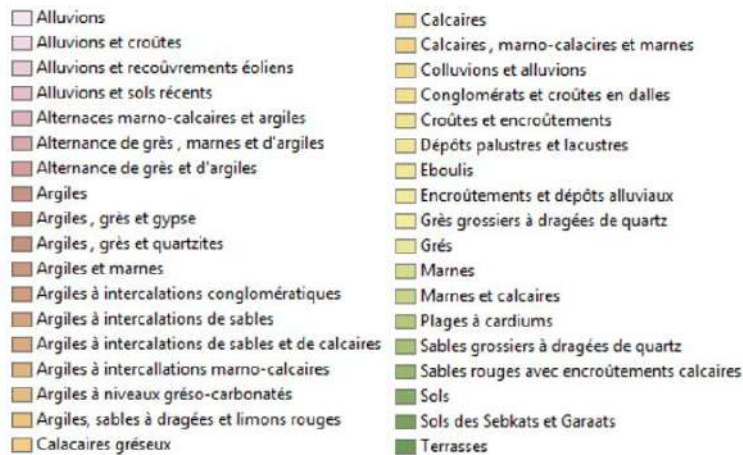
**Figure 26:** Vertical velocity from Sentinel 1 SBAS processing superimposed with a) delimitation of the aquifers; b) cropland mask; c) ground water wells; d) DEM (TanDEM-X).

It is observable that the areas of highest subsidence are situated within this mask, and seem to follow its border. This observation hints towards a subsidence caused by agricultural exploitation. This observation is supported by the analysis of the location of the ground water wells. Figure 26c shows the superimposition of the different ground water wells with the velocity field.





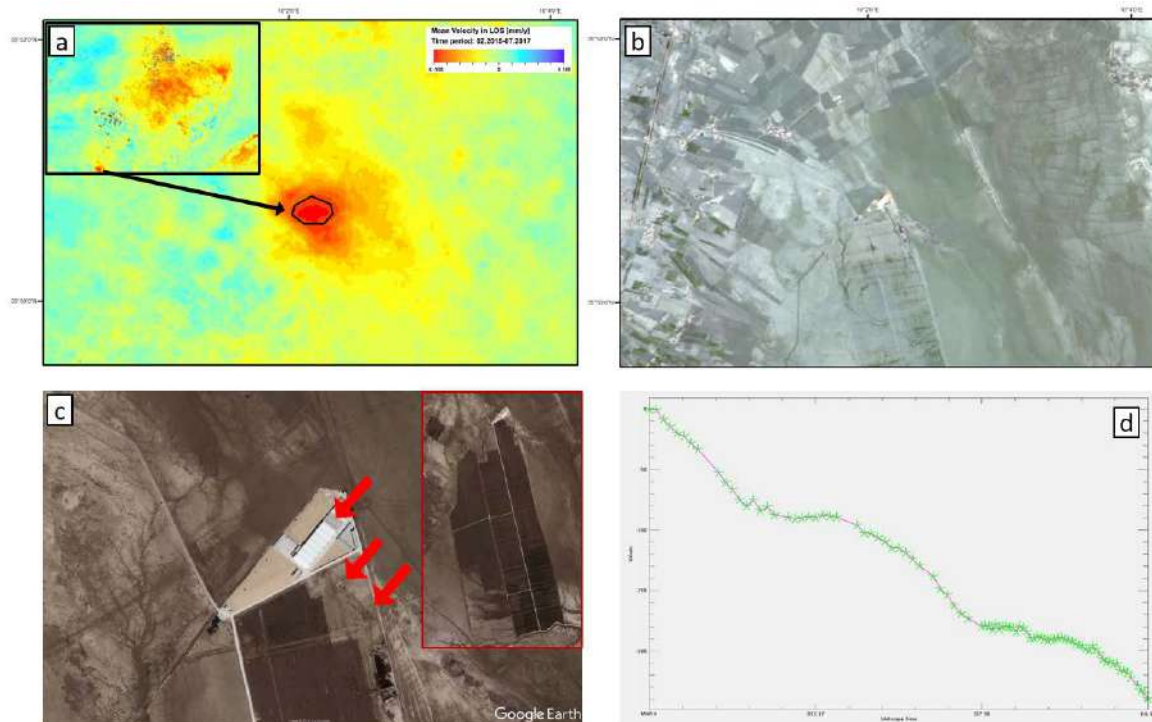




**Figure 27:** a) Vertical velocity from Sentinel 1 SBAS processing superimposed with the delimitation of the geological and lithological units; b) corresponding geological map; c) corresponding lithological map.

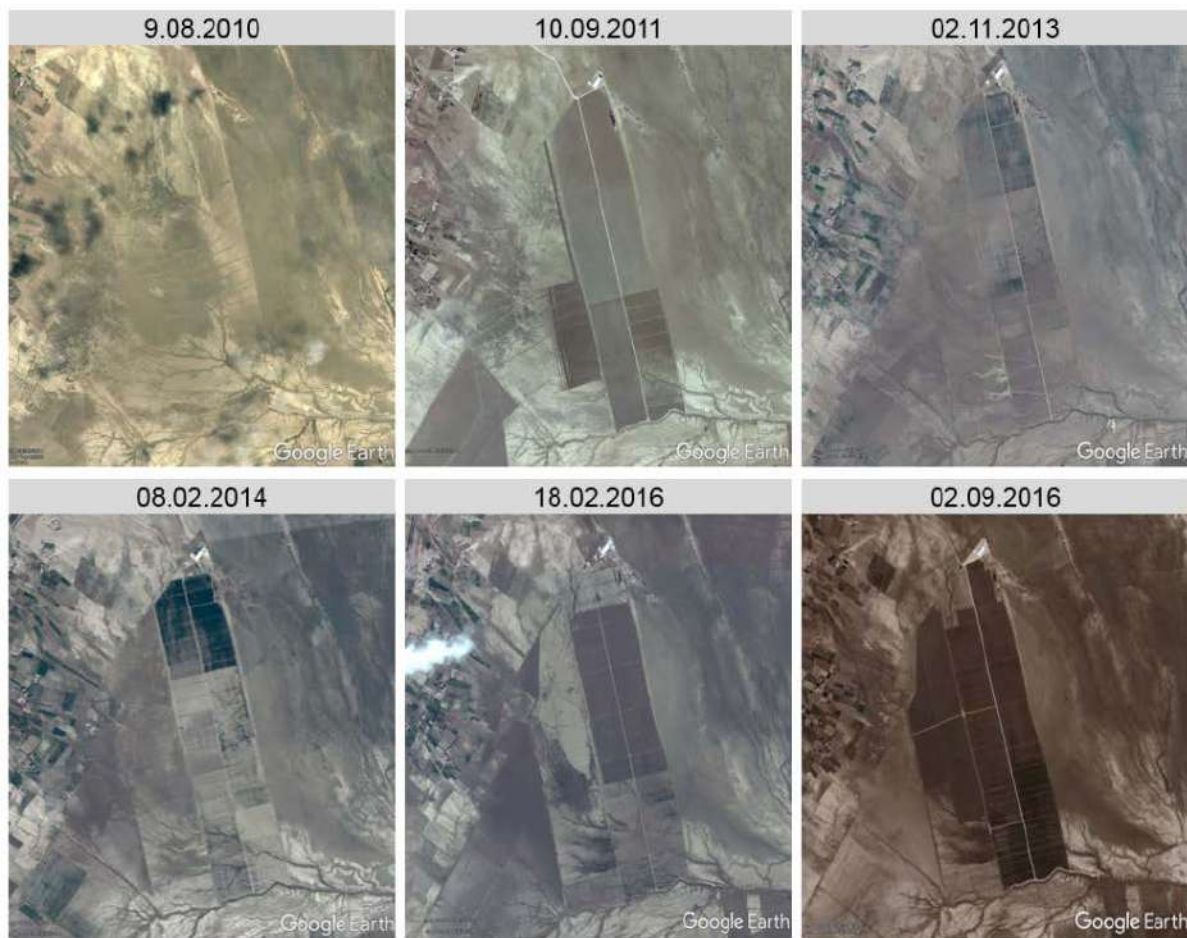
Those wells are principally used for irrigation and the water is directly pumped from the aquifer. There is a strong correlation between the location of the non-listed boreholes and the highest subsidence pattern. On the contrary, there is no visible correlation between the location of listed -and controlled- boreholes and the ground motion (red triangles, especially in the south west of the region). This indicates that the uncontrolled boreholes may contribute to a more intensive use of the ground water and thus to an overexploitation of the underlying aquifer.

A further analysis of the geographical, geological and lithological situation provides some additional explanation, which can substantiate the indication of an overexploitation of the aquifer. As from Figure 26d, the highest subsidence is observed on a relatively flat area. Some subsidence is also observable on the hills in the west part of the area. Those hillsides are higher, yet flat and used for agricultural purpose, mainly for tree plantations. Figure 27 shows that the main subsidence occurs on relatively new ground (quaternary, Figure 27b). The soil is composed by alluvial deposits (Figure 27c). Those sediments usually have a high compressibility and are therefore susceptible for higher ground compaction, especially through intensive water withdrawal in the underlying aquifer, which could explain the resulting subsidence of the upper ground.



**Figure 28:** a) Zoom to Sentinel 1 SBAS processing; b) corresponding satellite image; c) building in the centre of the deformation cluster; d) corresponding time series of main subsidence

Zooming in on particular areas, local small-scale deformation clusters are observable. Figure 28a shows one of this cluster, situated in the South-West of the original image extent. A comparison with optical data shows a strong correlation between the location of the subsidence cone and the position of a building (Figure 28a and 28b). This building is assumed to belong to a very important olive tree plantation, situated in the South of the building. A closer look at the building and its direct surroundings shows two possible ground water wells (red arrows in the bottom of Figure 28c). Additionally, using Google Earth time scale (Figure 29), it is noticeable, that those wells have been built recently (between 2010 and 2011), as has the building. Figure 28d shows the time series displacement of the area of main subsidence (shown in black line in Figure 28a), starting March 2015 and ending July 2017. Besides the obvious subsidence (about 100mm/a), a small seasonal pattern is recognizable, which indicates a small uplift during the winter months, which may correspond to ground water recharge. This should be further analysed, especially considering meteorological precipitation data. Thus, both the ground water over-extraction (volume reduction of the aquifer) and of minor importance the building load leading to soil compaction may cause the subsidence process here.

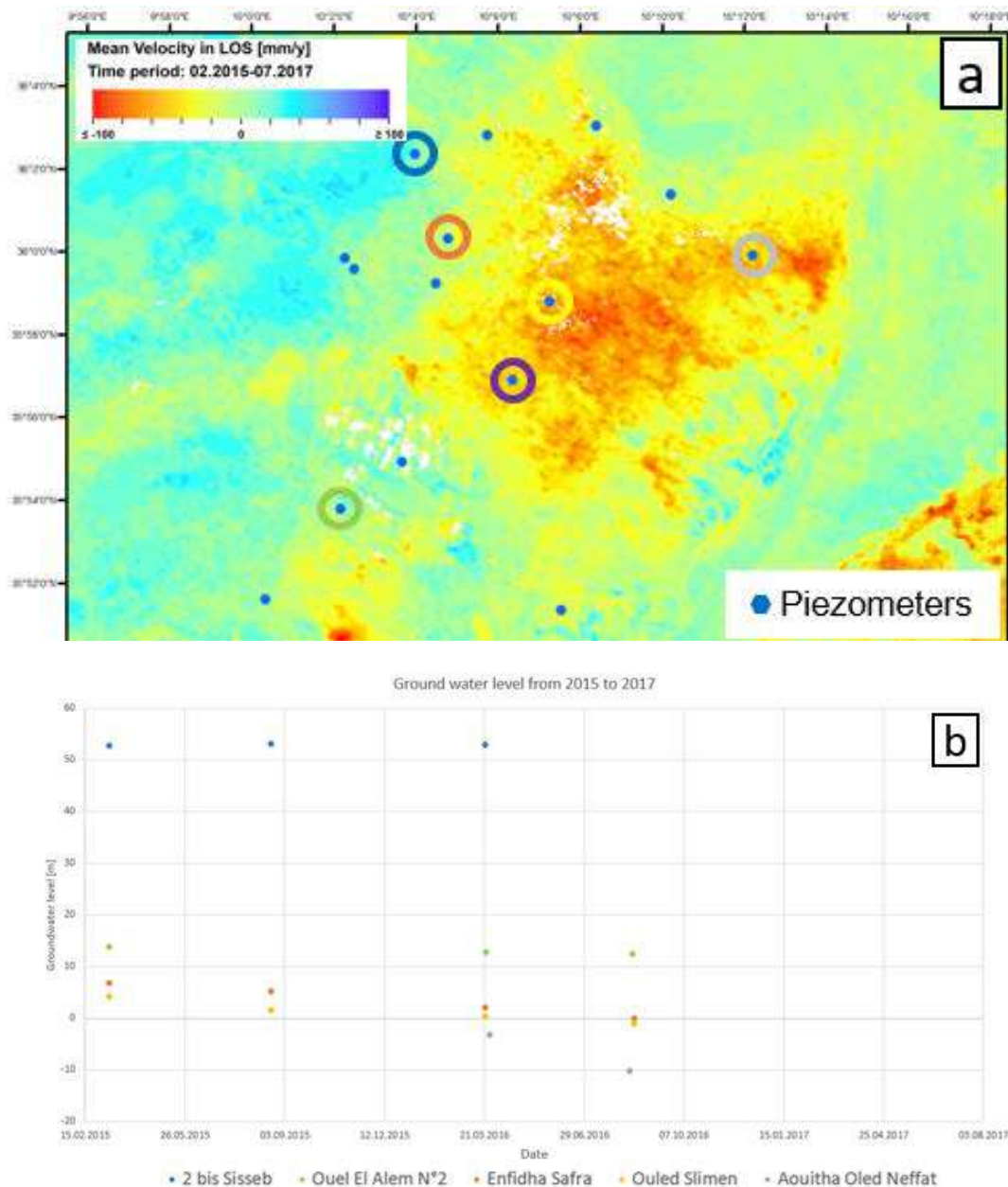


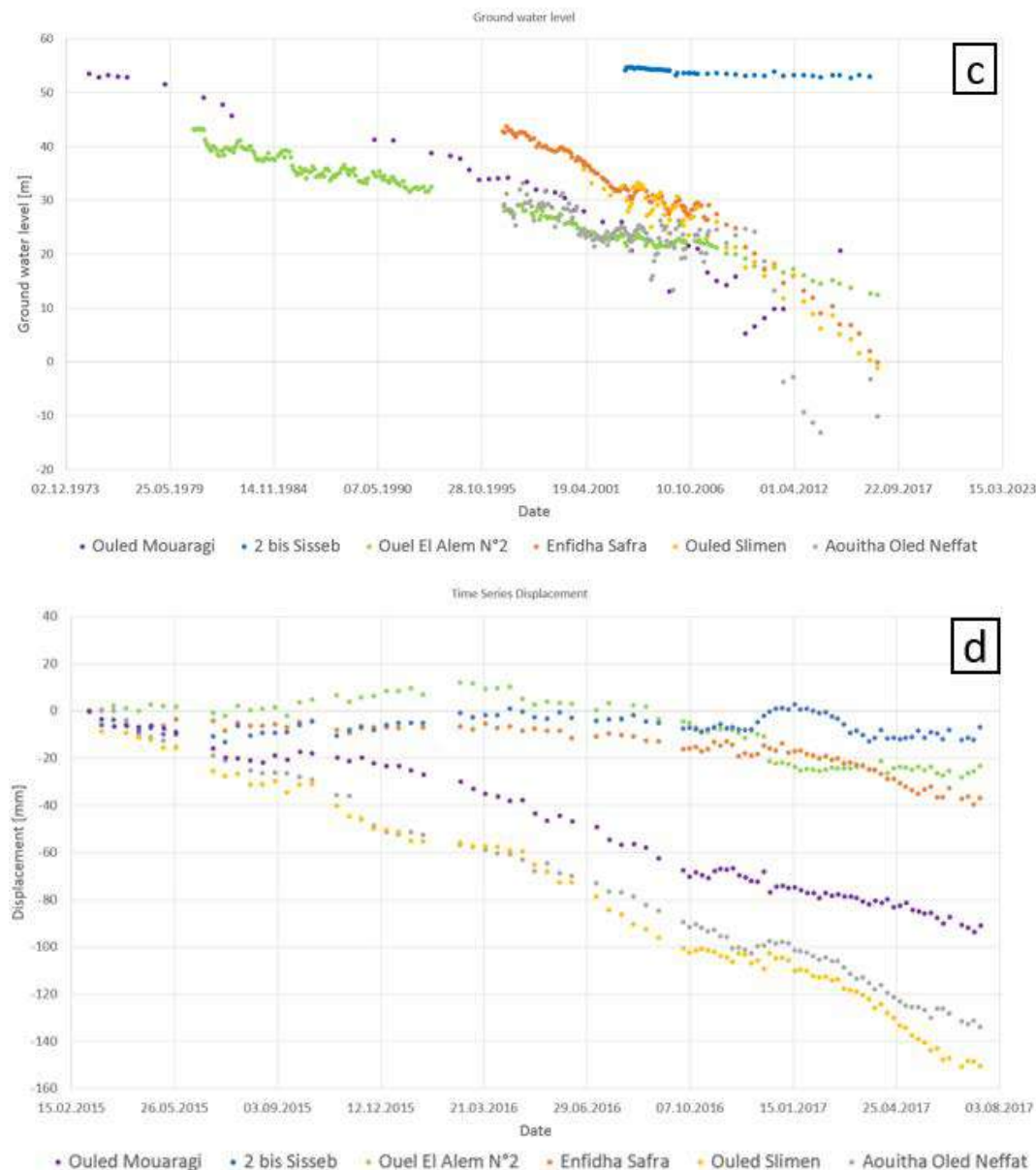
**Figure 29:** Multitemporal optical imagery (Google Earth 2018)

Figure 30 shows the evolution of the groundwater level at specific piezometers within and at the border of the main subsidence area. Figure 30a shows the geographical location of the piezometers. Figure 30b represents for selected piezometers the evolution of the ground water level during the timespan of the RADAR acquisitions (2015-2017), and Figure 30c the same since 1973. Unfortunately, there is no available ground water level information after 2016 so that only a linear trend can be assumed for 2017. Figure 30d shows the corresponding ground motion at each selected piezometer. The selected piezometers are encircled in Figure 30a and the same colour coding is used for all the sub-figures. Since 2008, only two groundwater level measurements per year are taken at the piezometers, in comparison to monthly measurements before. Furthermore, the measurements were made available until mid-2016, explaining the low amount of measurements in Figure 30b. For the piezometer Ouled Mouaragi (violet), no measurements are available since 2015. The following interpretation relies therefore strongly on the assumption that the trend of the groundwater levels since 1973 extends approximately linearly during the RADAR observation period. There seems to exist a correlation between the observed groundwater levels and the determined ground motion. At piezometers Ouled Slimen (yellow), Ouled Mouaragi (violet) and Aouitha Oled Neffat (grey) a strong subsidence is observed (-90 up to -150mm above the satellite observation periode). Also, a strong decrease of the ground water level is observed (a rough interpolation of Figure 30b and c would show a decrease of 10m up to more than 20m for the same time period). At piezometer 2 bis Sisseb (blue), the groundwater level is constant during the observation period (Figure 30b), which correlates with the observed ground motion (Figure 30d). In this case, the temporally denser information of the displacement even shows



a light uplift during winter 2016/2017, which could be due to a recharge of the aquifer through precipitation. This recharge is also visible at piezometers Ouled Slimen (yellow) and Aouitha Oled Neffat (grey). For piezometer Ouel El Alem N°2 (green), the decrease of the groundwater level is moderate (Figure 30b and c), as is the observed ground motion (Figure 30d). Finally, the groundwater level at piezometer Enfidha Safra (orange) shows a strongly decreasing trend, since 1996. The corresponding ground motion shows a rather stable ground from 2015 to 2016, the subsidence becoming evident towards the end of 2016/begin of 2017. Therefore, a certain correlation exists between the observed ground motion and the measured groundwater levels. Yet this correlation is not directly proportional, as it depends of many other factors such as e.g. soil properties and depth of the aquifer.





**Figure 30:** a) Geographical location of the piezometers from Sentinel 1 SBAS processing; b) evolution of the groundwater level for selected piezometers (2015-2017); c) evolution of the groundwater level for selected piezometers (since 1973); d) corresponding ground motion

All those maps indicate a strong correlation between the observed subsidence and a possible overexploitation of the underlying aquifer. On the other hand, all those explanations have to be considered with high care, as InSAR results are highly affected by difference of soil moisture, occurring particularly in agricultural areas. Thus, the observed motion pattern may indeed correspond to a subsidence, but this subsidence may not be as strong as shown or local velocity patterns may be caused by noise or other vegetation parameters inducing phase differences, not caused by ground motion.

More in-situ data are therefore necessary in order to corroborate this interpretation.

### 3.4 Transfer to DSS

A decision support system (DSS) has been developed for the Nebhana water system in the framework of the project. The DSS considers all aspects regarding the water cycle such as the drinking water supply, the surface runoff or the impacts on the hydrogeological system with the aim to facilitate the decision maker's daily work. It has been developed with the model system WEAP (Water Evaluation And Planning) which is an integrated tool to water resources planning, mainly for surface water. The WEAP system is linked to the groundwater modelling system MODFLOW in order to describe the groundwater flow dynamics.

Besides the global estimation of groundwater abstraction the classification approach, as it is shown in chapter 3.2, is used for the DSS.

#### 3.4.1 Data

One important input parameter is the land use and the crop classes, based on which the water consumption is then calculated. The goal is to simulate the crop irrigation requirements based on their reference evapotranspiration and, finally, to calculate the groundwater abstraction.

The same data are used for the classification as it was described in chapter 3.2. Input of InSAR analysis was discussed during the project stage (e.g. absolute ground motion data), but results of the InSAR analysis are not yet implemented in the DSS.

#### 3.4.2 Methodology

Five macro-classes have been identified for the land use classifications by optical data processing (chapter 3.2): cereals, forages, trees, vegetables and bare soil. As the goal of the DSS is to describe the water demand more in detail, these five classes are modified. Thus, the class trees is divided into olive trees, citrus trees and other trees (such as pomegranate and apricot tree). Olive trees may have a less water consumption compared to citrus trees over the year. This is also the case for citrus trees compared to other trees. Then, for the three tree classes (olive trees, citrus trees, other trees), the three annual crop classes (cereals, forages, vegetables) and the class bare soil, the land use with its corresponding crop type classes based on the developed classification approach (chapter 3.2) is calculated for both, summer and winter season (except cereals in the summer season).

The results of the classification approach show a low accuracy and a confusion for the crop classes olive trees and bare soil. These classes cannot be separated clearly in many cases. There is always a gap of bare soil or sometimes of grassland between each olive trees, which leads to mixed reflectance of bare soil and olive tree. This is also the case for bare soil with little vegetation cover such as weed. In order to face this problem and to improve the accuracy, a manual digitalisation of olive trees in the study area based on Google Earth satellite images is performed. This information is considered as the most reliable in terms of olive trees and the crop classification is calculated using this digitised layer (Figure 31).





**Figure 31:** Digitised olive tree layer

Rain-fed agriculture is practised in the Kairouan region, especially for olive trees. Studies and fieldwork show that almost 90% of the olive trees in the study area is rain-fed. As rain-fed agriculture does not demand irrigation water, this important aspect is considered in the DSS. Thus, the resulting class olive trees is further divided into rain-fed olive trees and irrigated olive trees (Table 7).

**Table 7:** Land use classes for the DSS

Olive trees - rain-fed	Citrus trees	Cereals	Vegetables
Olive trees - irrigated	Other trees	Forages	Bare soil

The water consumption and the corresponding crop irrigation requirements are then calculated using the MABIA extension tool of the WEAP model system. The MABIA method uses the dual crop coefficient method, as described in FAO Irrigation and Drainage Paper No. 56, whereby the dimensionless  $K_c$  value is divided into a basal crop coefficient,  $K_{cb}$ , and a separate component,  $K_e$ , representing evaporation from the soil surface. Available soil information derived from fieldwork is considered as well.

A schematic illustration of the components of the DSS is given in Figure 32.

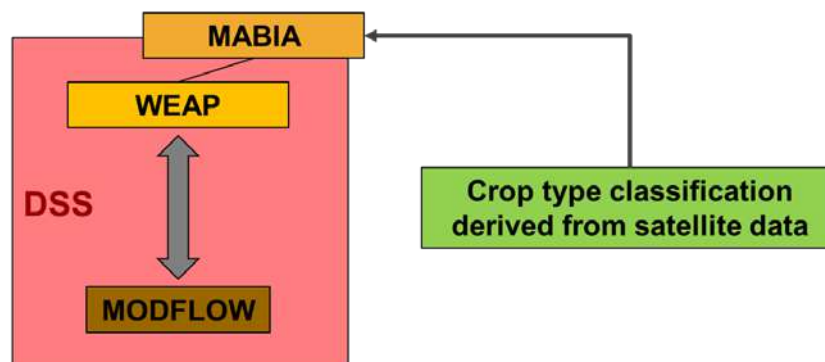


**Figure 32:** Schematic illustration of the components of the DSS

### 3.4.3 Results

Without using the digitised layer of olive trees, the crop type classifications for the seven classes in the winter season shows an overall accuracy of 70.6% and for the six classes in the summer season accordingly 80.2%. The relatively low accuracy, especially in the winter season, is mainly related to the confusion between olive trees and bare soil. Also, higher confusions can be observed by comparing all three classes to each other.

Figure 33 shows the resulting map of the crop type classification for the summer season for the study area of the DSS integrating the digitised olive tree layer (without differentiation of rain-fed and irrigated olive trees). Using the olive tree layer as a mask the overall accuracy can be significantly improved to a value of 89.4%.

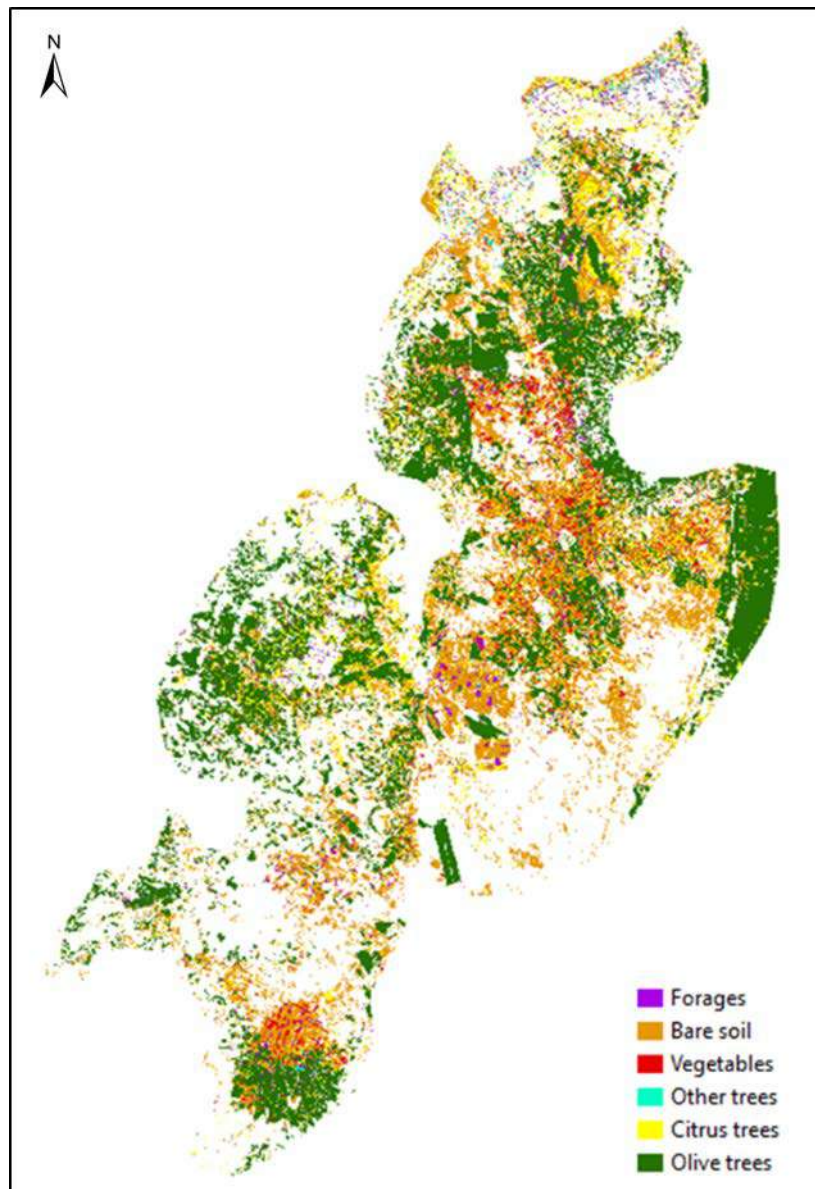


**Figure 33:** Crop type classification for the DSS

The results of the DSS and the estimated crop water needs are discussed in the project report by Nouri (2018).

## 4. Algeria

In Algeria, the study area is the plain of Remila-F'kirina, which is located in the eastern part of the country. As it is for Tunisia and Morocco, the focus is the quantification of groundwater volumes used for agricultural purposes and the increase of awareness about the overexploitation of the underlying aquifer systems. Furthermore, there is a high interest by the national water authorities to establish a database of the groundwater abstraction points.

### 4.1 Inventory of groundwater abstraction points

For the study area, an inventory of groundwater abstraction points exists, provided by the national water authorities in 2016. This inventory, containing information about the locations of the wells or boreholes, is obsolete and incorrect in many cases. Thus, an update of the inventory is necessary.

In order to create a new and reliable database of boreholes, the local authorities from the agriculture and water ministries (DSA and DRE) in cooperation with the regional river basin agency (ABH CSM) realised several weeks of fieldwork in the region during the last half of 2017. They collected the geo-coordinates of the groundwater abstraction points including, if possible, additional information of pumping rates and volumes as well as the corresponding irrigated surface based on farmer's declaration.

The fieldwork was validated and discussed afterwards with the relevant project partners during a working meeting. The result of the fieldwork and the meeting was a database of the location of the groundwater abstraction points, which is reliable, updated and shared with the national water authorities in Algeria by the project partner OSS.

In a further step, it is intended to compare the locations of the wells and boreholes with the irrigated areas that can be identified by satellite data. An intersection of these two layers allows a localisation of non-declared or non-inventoried groundwater abstraction points.

### 4.2 Optical Processing

This part presents the methodology developed for land cover classification and subsequent determination of crop water consumption for Algeria. It is based on the same methodology as for Tunisia, with slightly differences due to different final goals, identified during the training session that took place at BGR in Hannover in January and February of 2018.

#### 4.2.1 Data

As the methodology was adjusted during the training depending on the quality of the available reference data, different sets of data have been used. For the analysis of the NDVI profiles, a whole year (2017) has been considered. For the classification, the winter season 2016/2017 was considered in more details.

Table 8 shows the considered datasets. The grey fields represent the data that were taken into account for the winter classification.



**Table 8:** Overview of the acquired Sentinel-2 data.

Sentinel-2
16.02.2017
28.03.2017
17.04.2017
17.05.2017
26.06.2017
11.07.2017
05.08.2017
14.09.2017
14.10.2017
08.11.2017
08.12.2017

The ground truth data were acquired by local water authorities during the last half of 2017 (chapter 4.1). It consists mainly in an inventory of wells and boreholes and, if available, of the dedicated pumping rate or volume. However, it is not possible to allocate the wells to the corresponding agricultural areas in many cases. Thus, many of the training data need to be newly acquired, especially for the remote sensing task. During training, only reliable reference data were used, and new training areas have been defined using limited higher resolution imagery of Google Earth (tree plantations and bare soil).

#### 4.2.2 Methodology

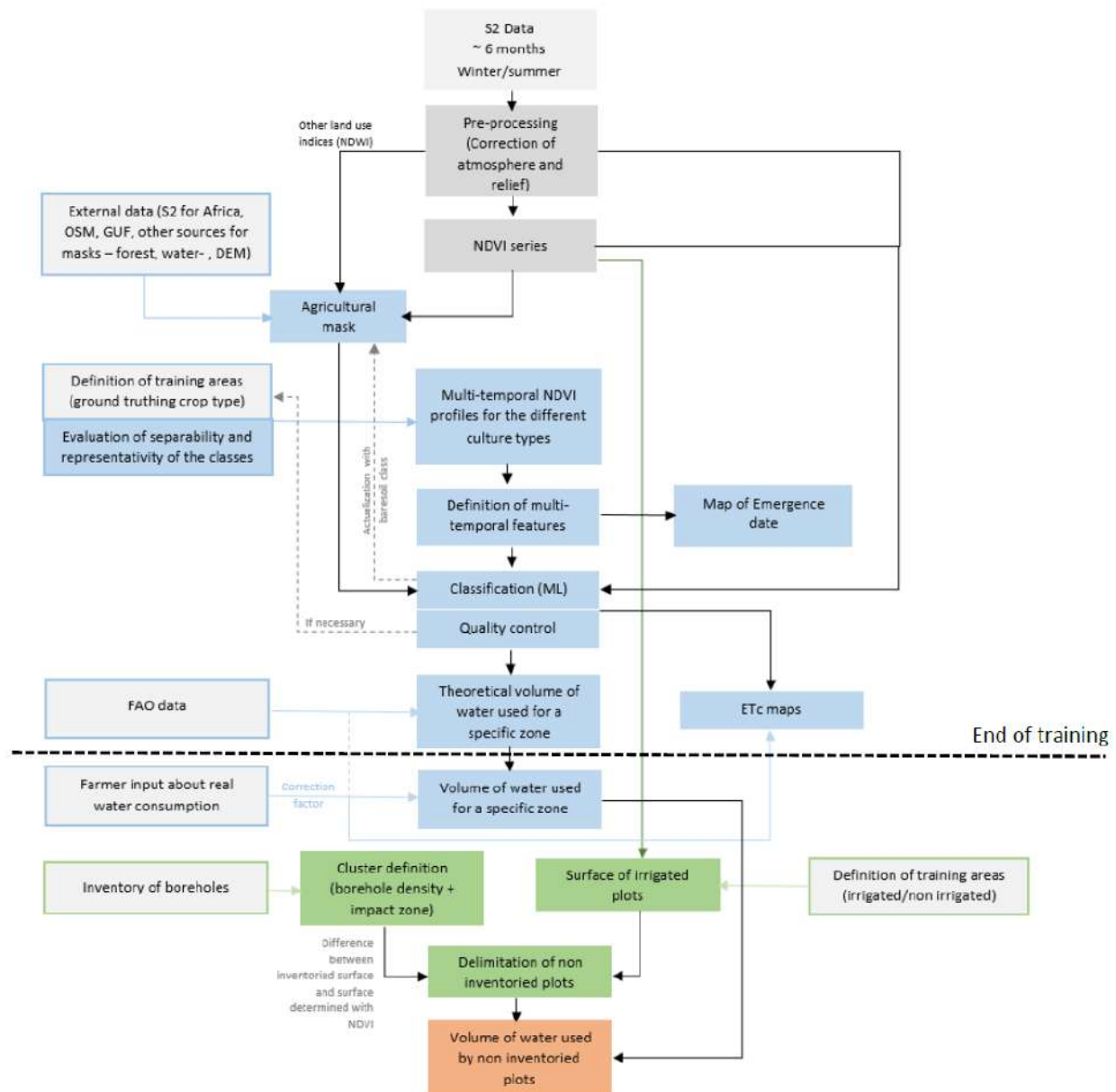
The workflow for the Algerian processing is presented in Figure 25. Three principal goals were identified and formulated during the training session:

1. Determine the water consumption of the pilot region
2. Determine the irrigated plots which are not inventoried
3. Determine the water consumption of the non-inventoried plots

The different steps necessary to achieve these goals are represented color-coded in Figure 34. Up to the dashed line, the workflow corresponds to the one for Tunisia and has been partly processed during the training. The remaining steps have still to be performed, but are explained here shortly. Using the FAO data and the developed excel tool, adjusted theoretical water needs are calculated. In order to determine the equivalent real water consumption, a correction factor can be defined, using in-situ data about the real water consumption. In order to fulfil the second goal, a thorough analysis of the NDVI time series needs to be conducted. Using reference data about irrigated and non-irrigated plots, a classification of irrigated and non-irrigated plots should be possible. Indeed, irrigated plots should show higher mean/max NDVI than non irrigated plots, and a more regular or “smoothed” NDVI profile as the non irrigated plots, who are more subject to precipitations. The determination of the total surface and location of the irrigated plots is then straightforward. Furthermore, using the existing inventory of boreholes, it is possible to delimitate the zone of influence of the listed boreholes, using buffering techniques. Therefore, the remaining surfaces that are not in those zone of influence of the inventoried boreholes characterize the plots that are irrigated by a non inventoried borehole. Using the previously determined water consumption together with the determined irrigated but non-inventoried plots, it is possible to determine the volume of water that is used by the non-inventoried plots, fulfilling the third goal.

## Goals:

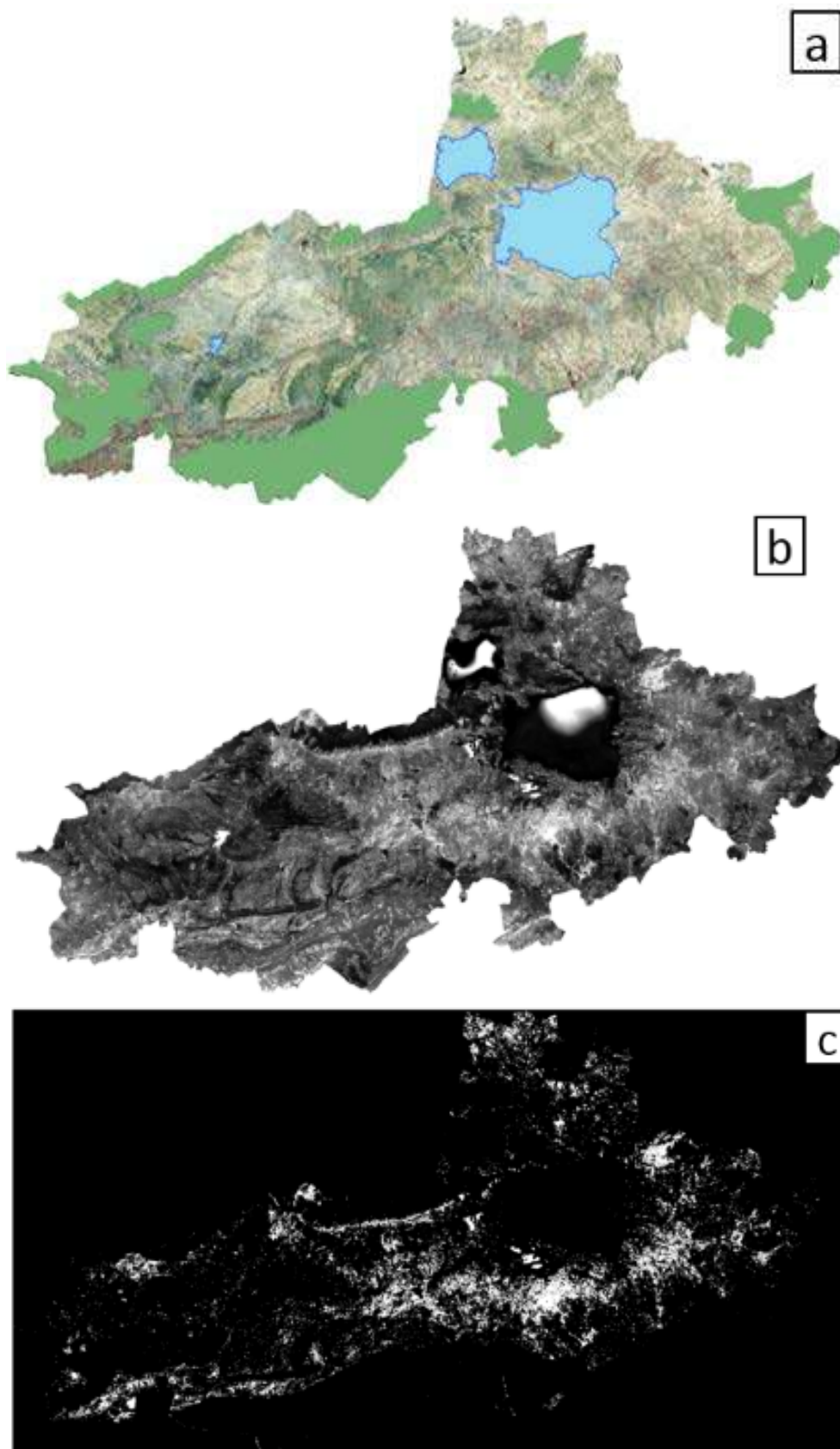
1. Determine the water consumption of the pilot region
2. Determine the irrigated plots which are not inventoried
3. Determine the water consumption of the non inventoried plots



**Figure 34:** Workflow for the processing of the Algerian sites

### 4.2.3 Results

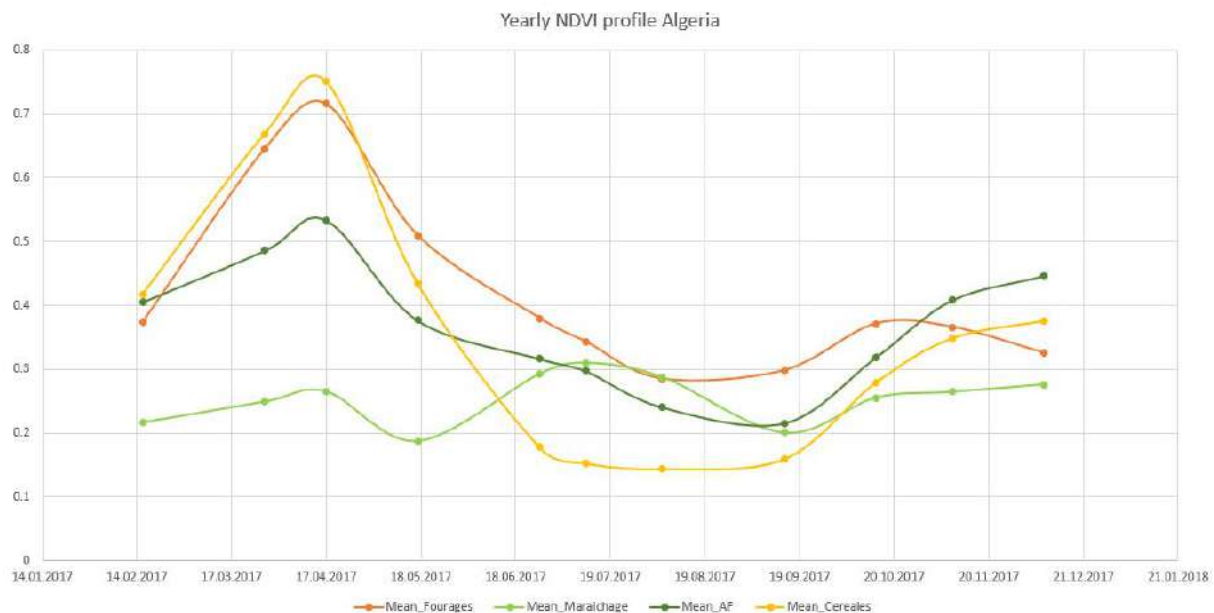
As for Algeria the available ESA CCI land cover – S2 prototype land cover 20m map of Africa 2016 (CCI Land Cover, 2017) is not satisfactory for the cropland mask, available external data in combination with multi-temporal NDVI analysis of the Sentinel 2 data for the year 2017 are used. The external data consist in a forest mask and a water mask created by the ABH. Additionally, a threshold on the standard deviation of the NDVI values of the Sentinel 2 time series is used. Figure 35 shows the external masks and the resulting cropland mask. The further analysis is performed without using the mask. Future work should include the use of the mask for crop mapping, in order to assess only relevant areas.



**Figure 35:** a) external data- blue: water mask, green: forest mask; b) standard deviation of NDVI over the year 2017; c) resulting cropland mask after thresholding

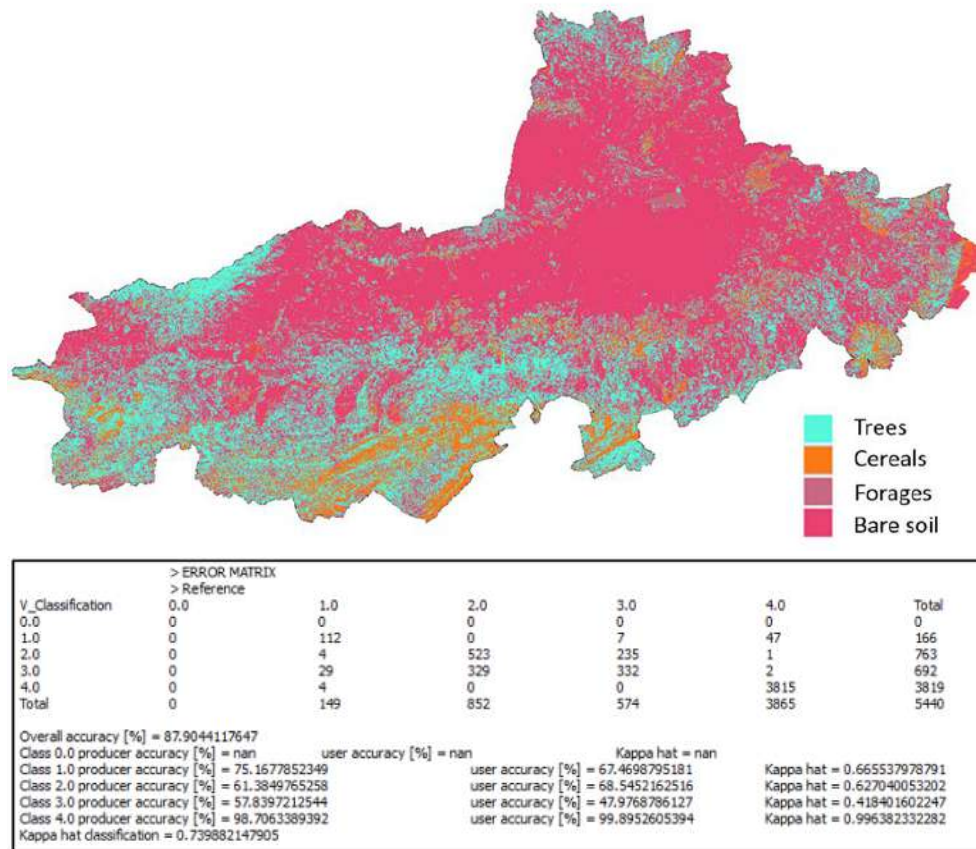


Figure 36 shows the NDVI profiles over the whole year 2017 using the available reference data of the pilot area in Algeria. The profiles are similar to those observed for Tunisia, so that the same multi-temporal features have been used. There, forages and cereals have the same growing period, whereas in Tunisia forages grow earlier than cereals (Figure 11b). In this case, it would be helpful to define additional multi-temporal features such as the date of harvesting, which seems to happen earlier for cereals as for forages, considering the NDVI profiles of Figure 36. However, as the reference data were not reliable for the differentiation between forages and cereals, the same features were used for classification as for Tunisia. For future work, it is recommended to investigate new and more reliable reference data and possibly define additional features.



**Figure 36:** NDVI Profiles for the year 2017 for four different crop types in Algeria.

The classification was performed on the Sentinel 2 scene of 17.04.2017, using 8 spectral bands (B2, B3, B4, B5, B6, B7, B8, B8a) and 3 additional multi-temporal bands (max NDVI, min NDVI, Difference minimum-maximum). Moreover, depending on the reference data and because very few vegetables grow in the area especially in winter, only four classes were considered: trees, cereals, forages and bare soil. The result is shown in Figure 37. It is necessary to mention that due to the large area, three different tiles needed to be mosaicked before processing.



**Figure 37:** Classification map and confusion matrix of the maximum likelihood classification for the plain of Remila

The confusion matrix shows an overall accuracy of almost 88%. A look at the producer's and user's accuracies shows that bare soil and trees are better classified than cereals and forages. Especially for bare soil, this is due to the fact that much more reliable training data were available (as defined using Google Earth). This overall result is therefore biased by the very good classification of the bare soil compared to the other classes. The use of better and reliable training data for the other classes should help to improve the overall classification. It should be then ensured that about the same amount of reference pixels is available for each class.

## 4.3 RADAR Processing

### 4.3.1 Data

For Algeria, only Sentinel 1 IW data were processed. Higher resolution is in this case not necessary, as large-scale motions should be observed. The large surface of the pilot area can be covered with a single data stack. Moreover, for Tunisia, a strong correlation was observed between TerraSAR-X and Sentinel 1 data, therefore Sentinel-1 data are found to be sufficient for further investigations, as the goal was the determination of large scale ground motion, and Sentinel 1 data are preferred for the sake of keeping the costs low. Table 9 resumes the number of available acquisitions for each dataset. A detailed overview of the acquired datasets and acquisition dates is given in Appendix 3.

**Table 9:** Number of available acquisitions and time span for each considered sensor

	Ascending	Descending
Sentinel 1	60 datasets, from 11.2014 to 05.2017	61 datasets, from 01.2015 to 05.2017

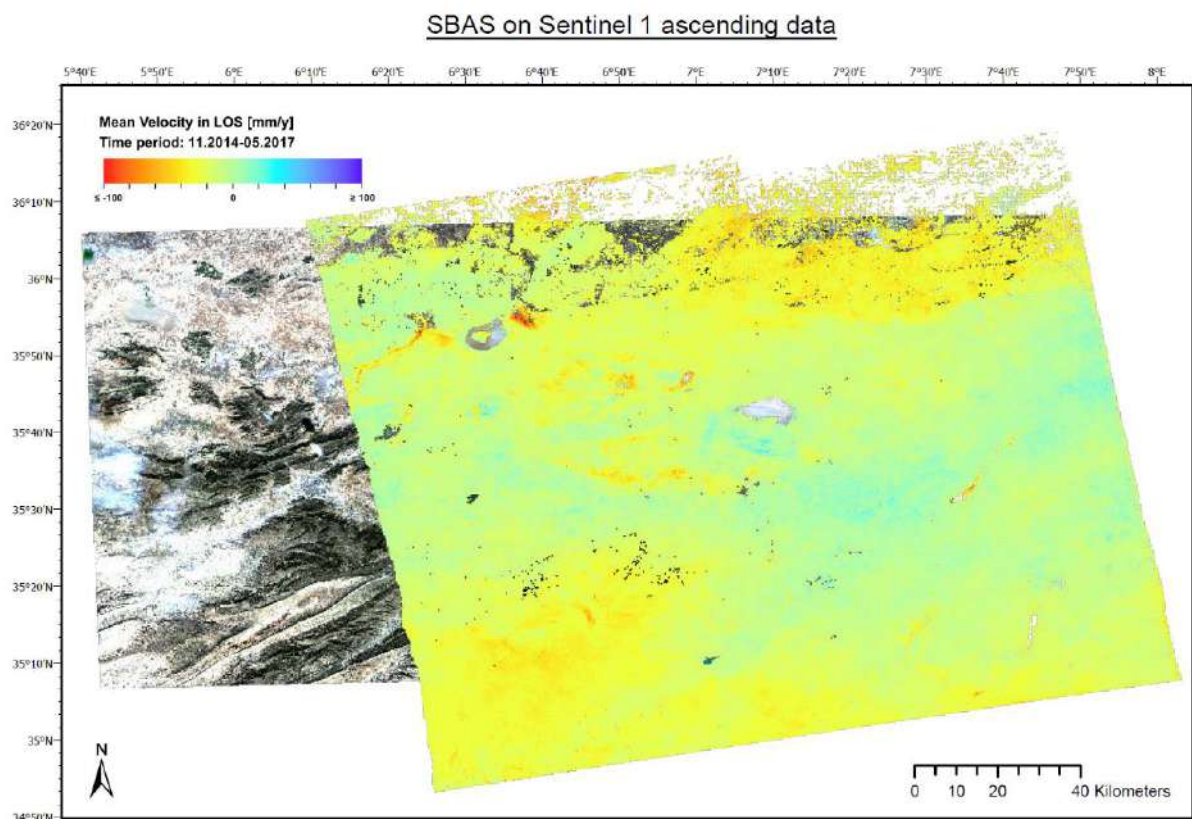
Only the ascending dataset was processed at the time of the report.

#### 4.3.2 Methodology

Considering the results obtained for Tunisia, the whole Sentinel 1 dataset in ascending direction was processed for Algeria using the SBAS technique. Indeed, due to the detection of distributed scatterers, this method provides more information about ground motion in rural areas than the PSI technique, which is of tremendous importance for the analysis of ground motion due to groundwater extraction in agricultural areas.

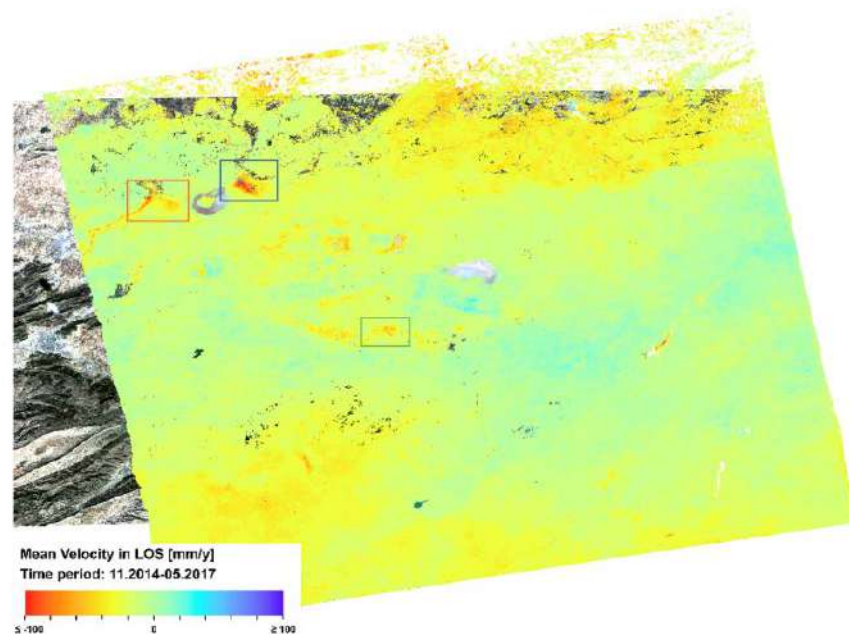
#### 4.3.3 Results and Interpretation

Figure 38 shows first results of the SBAS processing for Algeria. Strong local subsidence patterns are observable in the middle and in the north-western part of the considered frame. A closer comparison with a DEM shows that the more moderate regional subsidence patterns in the south and in the northern part are found in mountainous areas around the plain. The pattern in those areas may be caused by residual atmospheric or topographic phase inaccuracies and not by ground motion effects. Especially in the north, the subsidence pattern is not homogeneous and shows missing data at the upper border (very few scatterers compared to the rest of the frame). In order to provide a homogenized result, the SBAS processing should be performed anew by considering further data available in meantime.

**Figure 38:** SBAS result for the plain of Remila, Algeria, on Sentinel 1 ascending data.



The following interpretation is based on the presented, not reprocessed, first results, therefore it has to be considered carefully as it may contain some misinterpretation. The interpretation of local motion patterns relative to their direct surroundings is however possible and shown in the following for the areas situated in the middle and north-western part of the frame (coloured box in Figure 39). Those areas show a particularly strong subsidence relative to their direct surroundings.



**Figure 39:** Considered areas for the analysis.

A closer look at the corresponding areas in multispectral imagery (Figure 40) suggests the presence of multiple wells (red arrows and circles) in areas marked by strong subsidence (black boxes). Due to the resolution, this supposition should be confirmed with terrain verification. This would explain the subsidence due to important use of the groundwater, directly drawn from the aquifer in almost every single agricultural plot.

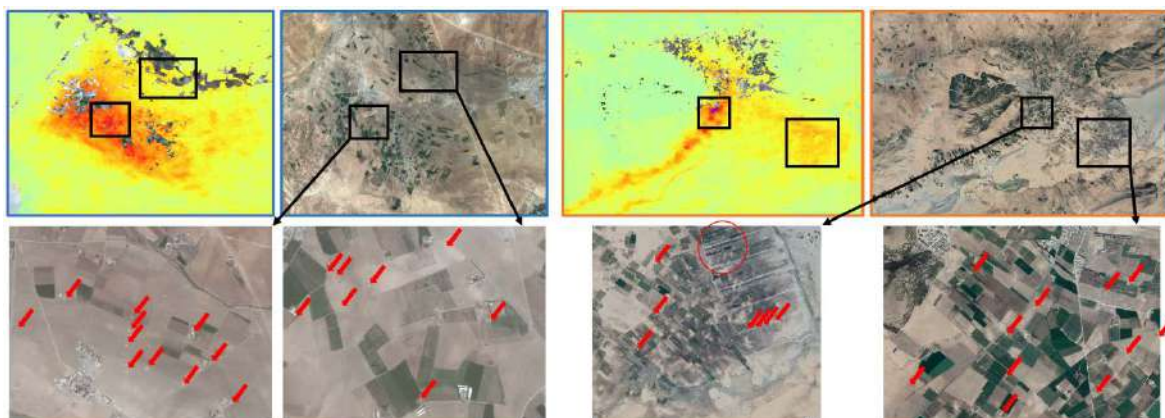


**Figure 40:** Zoom-up on selected areas and wells identification; source of optical imagery: Google Earth

An even closer look at these presumed wells is given in Figure 41 for the green area sketched in Figure 40. For each very local subsidence, one or more wells can be found in the direct vicinity of the main subsidence cone (marked by the coloured arrows). Those open wells are

quite big and well recognizable on high-resolution optical imagery (here Google Earth was used). They are mainly characterized by an almost perfect circle form, are dark in the middle and often surrounded by a quite bright (sandy) area. Therefore, it could be conceivable to use methods of automatic detection on high-resolution optical imagery to detect those wells. Here also, a terrain verification is needed to verify the presence of wells at those locations.

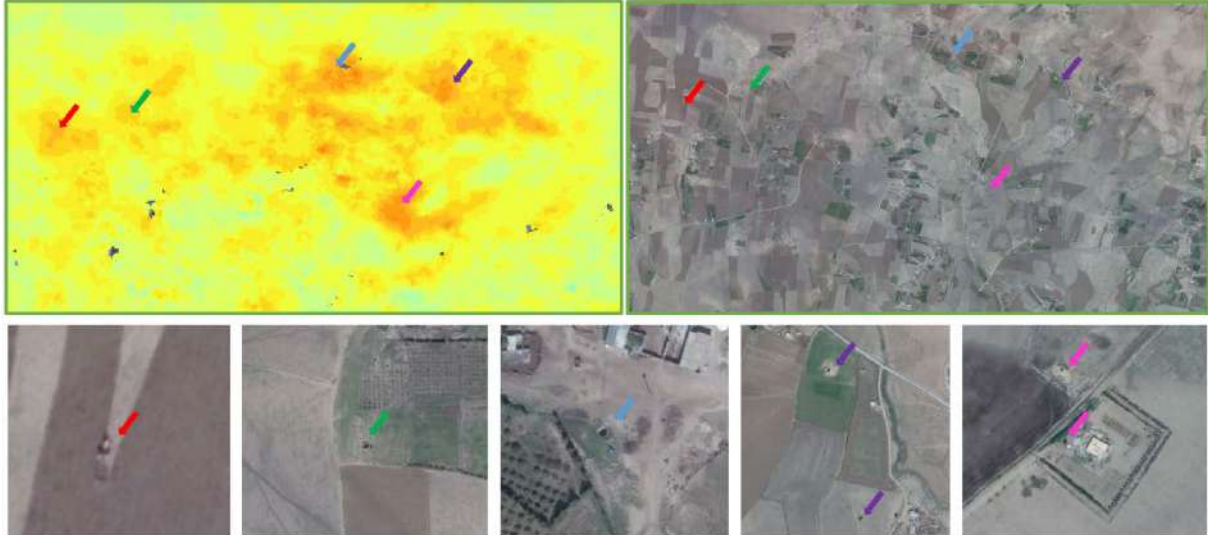


**Figure 41:** Closer look on presumed wells; source of optical imagery: Google Earth

## 5. Morocco

For Morocco, Sentinel 1 data are available for the pilot area since March 2015. Some data were downloaded and are listed in Appendix 4. No processing has been performed yet.



## 6. Representation of the project

### 6.1 Supervision of Internship students

During the project time, two internship students supported the project at BGR in Hannover.

The first student was at BGR for four weeks in September/ October 2016. Her goal was the analysis and correction of reference data for optical processing that were acquired during three different field campaigns in 2015. Her work contributed to visualize incoherent references and to reduce the number of crop classes for later ground truth acquisitions, through separability analysis.

The second student was at BGR for eight weeks in August/ September 2017. During this time, he performed statistical analysis of six months of newly acquired ground truth data, and contributed to the development of the multi-temporal features for classification. He also evaluated different classification methods and classification software. His work was an important contribution to this project.

### 6.2 Training of OSS

Capacity building is an important component of the technical cooperation. During a meeting at BGR with the OSS on 15 and 16 May 2017, it was decided to perform a high-level training for two OSS colleagues. The original training of one-month was planned for September 2017, but due to budget cut during the last half of the year 2017, this training was postponed to the period of 15 January 2018 to 9 February 2018. The goals of the training were multiple:

- Provide the colleagues with sufficient basic knowledge of remote sensing methods - it should encompass basic knowledge of both multispectral and RADAR remote sensing up to specific methodologies for determining water use by agriculture from remote sensing data
- Develop a method for the determination of water consumption with remote sensing data, respecting the specific goals of OSS and ABH
- Train the trainers

Training documents have been created and disseminated, and practical exercises have been performed using Copernicus data and available reference and external data. Additionally, each trainee documented the practical exercises in power-point presentations, which can serve with short adjustments as tutorials for future training.

### 6.3 Attendance of conferences

The following conferences relating to the project were attended:

- Zambia Water Forum and Exhibition (ZAWAFE), 12-13 June 2017, Lusaka, Zambia
- INSPIRE Conference 2017, 6-8 September 2017, Strasbourg, France
- 27th Colloquium of African Geology (CAG 27), 21-28 July 2018, Aveiro, Portugal

- ISPRS TC I Midterm Symposium Innovative Sensing – From Sensors to Methods and Applications, 10-12 October 2018, Karlsruhe, Germany (paper accepted)
- World Water Week 2019, 25-30 August 2019, Stockholm, Sweden.

A list of the corresponding presentations, abstracts or publications is given in the next section.

## 6.4 Publications

- Dubois, C., Bäumle, R., Himmelsbach, T. (2017) New Approaches of Remote Sensing for the Determination of Hidden Ground Water Bodies, Zambia Water Forum and Exhibition (ZAWAFE), 12-13 June 2017, Lusaka, Zambia (abstract + oral presentation)
- Dubois, C., Frei, M., Lege, T. (2017) Geospatial Copernicus Data and Standards: Applications in the International Technical Cooperation, INSPIRE Conference 2017, 6-8 September 2017, Strasbourg, France (abstract + oral presentation)
- Dubois, C., Stoffner, F., Frei, M. (2018) Methods of Remote Sensing for Assessing Groundwater Exploitation in the Maghreb Region, 27th Colloquium of African Geology (CAG 27), 21-28 July 2018, Aveiro, Portugal (abstract + poster presentation)
- Dubois, C., Stoffner, F., Sandner, M., Labiadh, M., Mimouni, M. (2018), Copernicus Sentinel-2 Data for the Determination of Groundwater Withdrawal in the Maghreb region, ISPRS TC I Midterm Symposium Innovative Sensing – From Sensors to Methods and Applications, 10-12 October 2018, Karlsruhe, Germany (peer-reviewed full paper + oral presentation, submitted)
- Stoffner, F., Krekeler, T., Mimouni, M., Ait Raoui, O., Aureli, A., Wende, F. (2019) Innovations in Groundwater Monitoring: Potential of Telemetry and Remote Sensing, World Water Week 2019, 25-30 August 2019, Stockholm, Sweden (oral presentation)

## 7. Conclusions and future work

In the beginning of the project, different classification approaches of crop types using commercial satellite data were tested in Tunisia. Due to the high dynamics and the different cultivation patterns, a detailed determination of crop types is difficult at single dates.

A methodology for estimating crop water needs based on Sentinel 2 remote sensing optical data has been set up and validated at the example of Tunisia, and still needs to be applied and possibly slightly adjusted regarding the specific needs in the study areas of Algeria and Morocco. Using land use classification of remote sensing optical imagery, the global water needs of very large areas can be estimated very quickly in a robust way.

This developed classification approach uses satellite data with an open data policy, allowing a sustainable use. In addition, the high repeatability rate is suitable for monitoring crop dynamics over time. All calculations can be done with freeware and/ or open source software.

An approach, which is proposed by the FAO, is used in order to estimate the crop water needs. Based on land use classification, the crop types are translated into theoretical water needs. In order to quantify the groundwater abstraction to adapt the approach for the specific cases, it will be necessary to consider relevant data such as soil data, precipitation data or irrigation patterns. Furthermore, a comparison of these results with real groundwater abstraction volumes, if available, would be of great benefit.

In Addition, the classification approach and its results were used as input for the DSS in order to estimate the water needs of different crop types.

RADAR Interferometry is a very useful technique to show an overexploitation of the groundwater resources as it allows visualizing over a large surface ground motions and their correlation with agricultural groundwater use. It is therefore a good tool for the detection of areas of over pumping and possibly for the detection of not listed wells or boreholes. As it is the case for the optical processing, a comparison with real groundwater abstraction volumes would be advantageous.

Capacity building has been performed during a high level training between BGR and OSS colleagues. Now that the methodology is developed, the local water authorities should be trained in remote sensing techniques as well as in GIS in order to apply this method and to adapt it for their specific future needs.

These activities, jointly conducted by OSS and BGR, fed into improving OSS's capacities in remote sensing techniques combined with agricultural perspectives in order to estimate groundwater abstraction and thus getting the project closer to achieving the mutual development aim.



## 8. References

- Allen, R. G., Pereira, L. S., Raes, D., & Smith, M., (1998): Crop evapotranspiration-Guidelines for computing crop water requirements-FAO Irrigation and drainage paper 56. FAO, Rome, 300(9), D05109.
- CCI Land Cover- S2 prototype land cover 20m Map of Africa 2016, ESA (2017): <http://2016africallandcover20m.esrin.esa.int/> (26.03.2018)
- Dubois, C., Stoffner, F., Sandner, M., Labiadh, M., Mimouni, M. (2018): Copernicus Sentinel-2 Data for the Determination of Groundwater Withdrawal in the Maghreb region, ISPRS TC I Midterm Symposium Innovative Sensing – From Sensors to Methods and Applications, 10-12 October 2018, Karlsruhe, Germany (peer-reviewed full paper + oral presentation, submitted)
- Nouiri, I. (2018): Modélisation WEAP du système hydrogéologique de Nebhana-Kairouan. Modèle conceptuel, données et résultats. Project report.

## Appendix 1 – Confusion matrix Tunisia

### Winter classification (Figure 13b)

V_Classification	> Reference					Total
	1.0	2.0	3.0	4.0	5.0	
1.0	3113	40	13	726	36	3928
2.0	39	10948	2748	516	99	14350
3.0	49	2282	9194	662	368	12555
4.0	2847	328	1482	20892	65	25614
5.0	52	44	254	368	1848	2566
Total	6100	13642	13691	23164	2416	59013

Overall accuracy [%] = 77.9404537983

Class 1.0 producer accuracy [%] = 51.0327868852

Class 2.0 producer accuracy [%] = 80.2521624395

Class 3.0 producer accuracy [%] = 67.1536045577

Class 4.0 producer accuracy [%] = 90.1916767398

Class 5.0 producer accuracy [%] = 76.4900662252

Kappa hat classification = 0.691646525244

user accuracy [%] = 79.2515274949

user accuracy [%] = 76.2926829268

user accuracy [%] = 73.2297889287

user accuracy [%] = 81.5647692668

user accuracy [%] = 72.0187061574

Kappa hat = 0.768595693319

Kappa hat = 0.691644463988

Kappa hat = 0.651429666398

Kappa hat = 0.696527582008

Kappa hat = 0.708242469825

### Summer Classification (Figure 13c)

V_Classification	> Reference					Total
	0.0	1.0	2.0	3.0	4.0	
0.0	0	0	0	0	0	0
1.0	0	1088	75	1721	50	2934
2.0	0	69	1785	369	71	2294
3.0	0	222	5	14913	8	15148
4.0	0	1522	575	1560	792	4449
Total	0	2901	2440	18563	921	24825

Overall accuracy [%] = 74.8358509567

Class 0.0 producer accuracy [%] = nan

Class 1.0 producer accuracy [%] = 37.504308859

Class 2.0 producer accuracy [%] = 73.1557377049

Class 3.0 producer accuracy [%] = 80.3372299736

Class 4.0 producer accuracy [%] = 85.993485342

Kappa hat classification = 0.510600681936

user accuracy [%] = nan

user accuracy [%] = 37.0824812543

user accuracy [%] = 77.8116826504

user accuracy [%] = 98.4486400845

user accuracy [%] = 17.801753203

Kappa hat = nan

Kappa hat = 0.287571883387

Kappa hat = 0.753931213668

Kappa hat = 0.938498067866

Kappa hat = 0.146347273788

### Summer Classification (Figure 13d)

V_Classification	> Reference					Total
	0.0	1.0	2.0	3.0	4.0	
0.0	0	0	0	0	0	0
1.0	0	2635	108	2764	33	5540
2.0	0	0	1967	92	62	2121
3.0	0	242	0	15600	4	15846
4.0	0	24	365	107	822	1318
Total	0	2901	2440	18563	921	24825

Overall accuracy [%] = 84.6888217523

Class 0.0 producer accuracy [%] = nan

Class 1.0 producer accuracy [%] = 90.8307480179

Class 2.0 producer accuracy [%] = 80.6147540984

Class 3.0 producer accuracy [%] = 84.0381403868

Class 4.0 producer accuracy [%] = 89.2508143322

Kappa hat classification = 0.685121585923

user accuracy [%] = nan

user accuracy [%] = 47.5631768953

user accuracy [%] = 92.7392739274

user accuracy [%] = 98.4475577433

user accuracy [%] = 62.3672230653

Kappa hat = nan

Kappa hat = 0.406246974287

Kappa hat = 0.91947843433

Kappa hat = 0.938455159657

Kappa hat = 0.609172654198

Summer Classification (Figure 13e)

V_Classification	> Reference	1.0	2.0	3.0	4.0	Total
0.0	0	0	0	0	0	0
1.0	0	2558	3	2603	28	5192
2.0	0	35	2176	140	63	2414
3.0	0	247	0	15727	6	15980
4.0	0	61	261	93	824	1239
Total	0	2901	2440	18563	921	24825

Overall accuracy [%] = 85.7401812689

Class 0.0 producer accuracy [%] = nan

user accuracy [%] = nan

Kappa hat = nan

Class 1.0 producer accuracy [%] = 88.1764908652

user accuracy [%] = 49.2681047766

Kappa hat = 0.425552226363

Class 2.0 producer accuracy [%] = 89.1803278689

user accuracy [%] = 90.1408450704

Kappa hat = 0.890661817678

Class 3.0 producer accuracy [%] = 84.7222970425

user accuracy [%] = 98.4167709637

Kappa hat = 0.937234652146

Class 4.0 producer accuracy [%] = 89.4679695983

user accuracy [%] = 66.5052461663

Kappa hat = 0.652147228948

Kappa hat classification = 0.704653608949

Summer Classification (Figure 13f)

V_Classification	> Reference	1.0	2.0	3.0	4.0	Total
0.0	0	0	0	0	0	0
1.0	0	2289	0	6380	61	8730
2.0	0	14	1833	92	11	1950
3.0	0	317	0	11976	5	12298
4.0	0	281	607	115	844	1847
Total	0	2901	2440	18563	921	24825

Overall accuracy [%] = 68.2457200403

Class 0.0 producer accuracy [%] = nan

user accuracy [%] = nan

Kappa hat = nan

Class 1.0 producer accuracy [%] = 78.9038262668

user accuracy [%] = 26.2199312715

Kappa hat = 0.164572976562

Class 2.0 producer accuracy [%] = 75.1229508197

user accuracy [%] = 94.0

Kappa hat = 0.933459906187

Class 3.0 producer accuracy [%] = 64.5154339277

user accuracy [%] = 97.3816880794

Kappa hat = 0.896199946615

Class 4.0 producer accuracy [%] = 91.6395222584

user accuracy [%] = 45.6957227937

Kappa hat = 0.436034269726

Kappa hat classification = 0.450614651212

Summer Classification (Figure 13g)

V_Classification	> Reference	1.0	2.0	3.0	4.0	Total
0.0	0	0	0	0	0	0
1.0	0	1775	237	1810	26	3848
2.0	0	33	1785	50	88	1956
3.0	0	1093	0	16550	16	17659
4.0	0	0	418	153	791	1362
Total	0	2901	2440	18563	921	24825

Overall accuracy [%] = 84.1933534743

Class 0.0 producer accuracy [%] = nan

user accuracy [%] = nan

Kappa hat = nan

Class 1.0 producer accuracy [%] = 61.1857980007

user accuracy [%] = 46.1278586279

Kappa hat = 0.389994567796

Class 2.0 producer accuracy [%] = 73.1557377049

user accuracy [%] = 91.2576687117

Kappa hat = 0.903047409322

Class 3.0 producer accuracy [%] = 89.1558476539

user accuracy [%] = 93.71991619

Kappa hat = 0.75103308754

Class 4.0 producer accuracy [%] = 85.884907709

user accuracy [%] = 58.0763582966

Kappa hat = 0.564610774228

Kappa hat classification = 0.640920969025

Summer Classification (Figure 13h)

V_Classification	> Reference	1.0	2.0	3.0	4.0	Total
0.0	0	0	0	0	0	0
1.0	0	1999	202	3250	11	5462
2.0	0	37	1885	74	122	2118
3.0	0	847	0	15072	15	15934
4.0	0	18	353	167	773	1311
Total	0	2901	2440	18563	921	24825

Overall accuracy [%] = 79.472306143

Class 0.0 producer accuracy [%] = nan

user accuracy [%] = nan

Kappa hat = nan

Class 1.0 producer accuracy [%] = 68.907273354

user accuracy [%] = 36.5983156353

Kappa hat = 0.282089575646

Class 2.0 producer accuracy [%] = 77.2540983607

user accuracy [%] = 88.9990557129

Kappa hat = 0.877999355852

Class 3.0 producer accuracy [%] = 81.1937725583

user accuracy [%] = 94.5901845111

Kappa hat = 0.785533903686

Class 4.0 producer accuracy [%] = 83.9305103149

user accuracy [%] = 58.9626239512

Kappa hat = 0.573814901099

Kappa hat classification = 0.575870322224



## Appendix 2 – Data Tunisia

<b>TerraSAR-X, ascending</b>	<b>ENVISAT ASAR, descending</b>
14.12.2015	24.09.2003
25.12.2015	21.04.2004
05.01.2016	26.05.2004
16.01.2016	04.08.2004
27.01.2016	13.10.2004
07.02.2016	17.11.2004
18.02.2016	22.12.2004
29.02.2016	26.01.2005
11.03.2016	02.03.2005
22.03.2016	06.04.2005
02.04.2016	11.05.2005
13.04.2016	24.08.2005
24.04.2016	02.11.2005
16.05.2016	11.01.2006
07.06.2016	15.02.2006
	22.03.2006
	31.05.2006
	18.10.2006
	27.12.2006
	31.01.2007
	11.03.2009
	22.09.2010

<b>Sentinel 1, ascending – track 88</b>				
04.03.2015	29.12.2015	06.10.2016	15.02.2017	03.07.2017
16.03.2015	10.01.2016	12.10.2016	21.02.2017	09.07.2017
28.03.2015	22.01.2016	18.10.2016	27.02.2017	15.07.2017
09.04.2015	15.02.2016	24.10.2016	05.03.2017	
21.04.2015	27.02.2016	30.10.2016	11.03.2017	
03.05.2015	10.03.2016	05.11.2016	17.03.2017	
15.05.2015	22.03.2016	11.11.2016	23.03.2017	
27.05.2015	03.04.2016	17.11.2016	29.03.2017	
02.07.2015	15.04.2016	23.11.2016	04.04.2017	
14.07.2015	27.04.2016	29.11.2016	10.04.2017	
26.07.2015	09.05.2016	05.12.2016	16.04.2017	
07.08.2015	21.05.2016	11.12.2016	22.04.2017	
19.08.2015	02.06.2016	17.12.2016	28.04.2017	
31.08.2015	14.06.2016	23.12.2016	04.05.2017	
12.09.2015	08.07.2016	29.12.2016	10.05.2017	
24.09.2015	20.07.2016	04.01.2017	16.05.2017	
06.10.2015	01.08.2016	10.01.2017	22.05.2017	
30.10.2015	13.08.2016	16.01.2017	28.05.2017	
11.11.2015	25.08.2016	22.01.2017	03.06.2017	
23.11.2015	06.09.2016	28.01.2017	09.06.2017	
05.12.2015	18.09.2016	03.02.2017	15.06.2017	
17.12.2015	30.09.2016	09.20.2017	27.06.2017	

<b>Sentinel 1, descending – track 95</b>			
09.02.2015	04.02.2016	25.10.2016	18.03.2017
21.02.2015	16.02.2016	31.10.2016	24.03.2017
05.03.2015	28.02.2016	06.11.2016	30.03.2017
17.03.2015	11.03.2016	12.11.2016	05.04.2017
29.03.2015	04.04.2016	18.11.2016	11.04.2017
10.04.2015	16.04.2016	24.11.2016	17.04.2017
22.04.2015	28.04.2016	30.11.2016	23.04.2017
04.05.2015	10.05.2016	06.12.2016	29.04.2017
16.05.2015	22.05.2016	12.12.2016	05.05.2017
09.06.2015	03.06.2016	18.12.2016	11.05.2017
03.07.2015	15.06.2016	24.12.2016	17.05.2017
15.07.2015	09.07.2016	30.12.2016	23.05.2017
08.08.2015	21.07.2016	05.01.2017	29.05.2017
20.08.2015	02.08.2016	11.01.2017	04.06.2017
13.09.2015	14.08.2016	23.01.2017	10.06.2017
31.10.2015	26.08.2016	29.01.2017	16.06.2017
24.11.2015	07.09.2016	04.02.2017	22.06.2017
06.12.2015	19.09.2016	16.02.2017	28.06.2017
18.12.2015	01.10.2016	22.02.2017	04.07.2017
30.12.2015	07.10.2016	28.02.2017	10.07.2017
11.01.2016	13.10.2016	06.03.2017	
23.01.2016	19.10.2016	12.03.2017	

## Appendix 3 – Data Algeria

Sentinel 1, ascending – track 161					
21.11.2014	20.05.2015	15.01.2016	14.05.2016	23.09.2016	21.01.2017
03.12.2014	01.06.2015	27.01.2016	26.05.2016	05.10.2016	02.02.2017
13.02.2015	13.06.2015	08.02.2016	07.06.2016	17.10.2016	14.02.2017
25.02.2015	25.06.2015	20.02.2016	01.07.2016	29.10.2016	26.02.2017
09.03.2015	07.07.2015	03.03.2016	13.07.2016	10.11.2016	10.03.2017
21.03.2015	16.11.2015	15.03.2016	25.07.2016	22.11.2016	22.03.2017
02.04.2015 (2)	28.11.2015	27.03.2016	06.08.2016	04.12.2016	03.04.2017
14.04.2015	10.12.2015	08.04.2016	18.08.2016	16.12.2016	15.04.2017
26.04.2015	22.12.2015	20.04.2016	30.08.2016	28.12.2016	27.04.2017
08.05.2015	03.01.2016	02.05.2016	11.09.2016	09.01.2017	09.05.2017

Sentinel 1, descending – track 66						
02.01.2015	08.05.2016	17.09.2016	22.11.2016	21.01.2017	28.03.2017	27.05.2017 (2)
21.01.2016 (2)	20.05.2016 (2)	29.09.2016	28.11.2016	27.01.2017	03.04.2017	
02.02.2016 (2)	01.06.2016	05.10.2016	04.12.2016	02.02.2017	09.04.2017	
14.02.2016 (2)	13.06.2016	11.10.2016	10.12.2016	08.02.2017	15.04.2017	
26.02.2016	07.07.2016	17.10.2016	16.12.2016	14.02.2017 (2)	21.04.2017	
09.03.2016 (2)	19.07.2016	23.10.2016	22.12.2016	20.02.2017	27.04.2017	
21.03.2016	31.07.2016 (2)	29.10.2016	28.12.2016	26.02.2017 (2)	03.05.2017	
02.04.2016 (2)	12.08.2016	04.11.2016	03.01.2017	04.03.2017	09.05.2017	
14.04.2016	24.08.2016	10.11.2016	09.01.2017	10.03.2017	15.05.2017	
26.04.2016 (2)	05.09.2016	16.11.2016	15.01.2017	16.03.2017	21.05.2017	

## Appendix 4 – Data Morocco

Sentinel 1, descending – track 52						
14.03.2015	29.08.2015					
26.03.2015	10.09.2015					
07.04.2015						
01.05.2015						
13.05.2015						
25.05.2015						
06.06.2015						
18.06.2015						
30.06.2015						
17.08.2015						